Low-energy nuclear spectroscopy in a microscopic multiphonon approach

2012 J. Phys. G: Nucl. Part. Phys. 39 043101

(http://iopscience.iop.org/0954-3899/39/4/043101)

J. Phys. G: Nucl. Part. Phys. **39** (2012) 043101 (37pp) doi:10.1088/0954-3899/39/4/043101

TOPICAL REVIEW

Low-energy nuclear spectroscopy in a microscopic multiphonon approach

N Lo Iudice[1], V Yu Ponomarev[2], Ch Stoyanov[3], A V Sushkov[4] and V V Voronov[4]

[1] Dipartimento di Scienze Fisiche, Università di Napoli Federico II and INFN Sezione di Napoli, Napoli, Italy
[2] Institut für Kernphysik, TU-Darmstadt, Schlossgartenstrasse 9, D-64289 Darmstadt, Germany
[3] Institute for Nuclear Research and Nuclear Energy, Bulgarian Academy of Sciences, 1784 Sofia, Bulgaria
[4] Bogoliubov Laboratory of Theoretical Physics, Joint Institute for Nuclear Research, 141980 Dubna, Russia

E-mail: loiudice@na.infn.it

Received 22 December 2011
Published 5 March 2012
Online at stacks.iop.org/JPhysG/39/043101

Abstract
The low-lying spectra of heavy nuclei are investigated within the quasiparticle–phonon model. This microscopic approach goes beyond the quasiparticle random-phase approximation by treating a Hamiltonian of separable form in a microscopic multiphonon basis. It is therefore able to describe the anharmonic features of collective modes as well as the multiphonon states, whose experimental evidence is continuously growing. The method can be put in close correspondence with the proton–neutron interacting boson model. By associating the microscopic isoscalar and isovector quadrupole phonons with proton–neutron symmetric and mixed-symmetry quadrupole bosons, respectively, the microscopic states can be classified, just as in the algebraic model, according to their phonon content and their symmetry. In addition, these states disclose the nuclear properties which are to be ascribed to genuine shell effects, not included in the algebraic approach. Due to its flexibility, the method can be implemented numerically for systematic studies of spectroscopic properties throughout entire regions of vibrational nuclei. The spectra and multipole transition strengths so computed are in overall good agreement with the experimental data. By exploiting the correspondence of the method with the interacting boson model, it is possible to embed the microscopic states into this algebraic frame and, therefore, face the study of nuclei far from shell closures, not directly accessible to merely microscopic approaches. Here, it is shown how this task is accomplished through systematic investigations of magnetic dipole and, especially, electric dipole modes along paths moving from the vibrational to the transitional regions. The method is very well suited to the study of well-deformed nuclei. It provides reliable descriptions of low-lying

magnetic as well as electric multipole modes of nuclei throughout the rare-earth and actinide regions. Attention is focused here on the low-lying 0^+ states produced in large abundance in recent experiments. The analysis shows that the quasiparticle–phonon model accounts for the occurrence of so many 0^+ levels and discloses their nature.

(Some figures may appear in colour only in the online journal)

1. Introduction

Multiphonon collective modes in nuclei were already predicted within the Bohr–Mottelson model [1]. Their evidence, however, has grown considerably in the last two decades. At low energy, fluorescence scattering experiments have detected low-lying double–quadrupole, double–octupole and mixed quadrupole–octupole multiplets in nearly spherical heavy nuclei [2–4]. At high energy, reaction experiments have established the existence of a double giant dipole resonance (GDR) [5, 6].

The discovery of these complex spectra has stimulated several theoretical studies in different approaches. The proton–neutron ($\pi - \nu$) interacting boson model (IBM2) [7] came out to be a precious tool for a systematic analysis of low-energy spectra throughout the whole periodic table. The IBM2 is able to classify the states according to their symmetry and show how the gross properties of nuclei evolve as one moves from spherical to transitional and, eventually, well-deformed regions. Because of its phenomenological nature, however, the IBM2 cannot unveil the fine structure of collective modes. These need to be studied in approaches that explicitly consider the nucleonic degrees of freedom.

The particle–hole (ph) random-phase approximation (RPA) and its quasiparticle (qp) version (QRPA) are perhaps the most widely adopted microscopic approaches to collective motion in nuclei [8, 9]. The QRPA, for instance, not only explains the global properties of collective modes but also accounts for the fragmentation induced by the single-particle levels (Landau damping) [10]. It relies, however, on a harmonic approximation and, therefore, cannot account for the collisional damping, responsible for the so-called spreading width, and is unable to describe multiphonon spectra and their anharmonic features.

The RPA can be extended so as to include the two-particle two-hole (2p2h) states. This extension in the small-amplitude limit is known as the second RPA (SRPA). The SRPA equations were derived first by Sawicki [11] and later by Yannouleas *et al* [12, 13] using the equations of motion method of Rowe [14]. Their solution in finite nuclei is quite problematic and, therefore, requires more or less severe approximations.

The most drastic one is to neglect the mutual coupling among 2p2h states [15, 16] as in recent calculation based on the unitary correlation method [17]. A more refined approximation consists in replacing one ph pair with a correlated state (RPA phonons) thereby obtaining a particle–phonon coupling [1, 18–21]. A further step was made in SRPA calculations using a Skyrme force [22–24], where the interaction between 2p2h states is partly taken into account.

The relativistic RPA plus phonon coupling (PC) [25, 26] relies on equivalent approximations. It is based on the Migdal theory, which exploits the Green function techniques to enlarge the configuration space beyond the ph space underlying the RPA [27]. An upgraded version, based on modern extensions of the Landau–Migdal theory [28, 29], was developed recently [30, 31]. This new formulation, dubbed as relativistic quasiparticle time blocking approximation, uses the quasiparticle formalism and treats consistently the quasiparticle–phonon coupling.

All the above approaches include up to two ph or qp phonons. Thus, they can account for the fragmentation of the resonances but are not suited to the description of multiphonon collective modes, especially at low energy.

An equations of motion phonon method, proposed recently [32, 33], iteratively generates a multiphonon basis and formulates an exact eigenvalue problem within the space spanned by such a basis. Its numerical implementation on ^{16}O within a space covering up to three-phonon states has pointed out the strong impact of the multiphonon states on spectra and transitions.

Most of the approaches mentioned above adopt realistic Hamiltonians and, therefore, are not flexible enough to be used for systematic studies. They are, in fact, adopted mostly for investigating the fine structure of giant and pygmy resonances.

The quasiparticle–phonon model (QPM) [34] is, to our knowledge, the only microscopic extension of QRPA that is suited to the study of low-energy spectra and high-energy responses. The QPM adopts a two-body Hamiltonian which is a sum of several separable multipole–multipole potentials. Due to this simplifying assumption, the QPM is able to cover a very large configuration space and to include up to three-phonon basis states.

Because of its handiness, the QPM is widely adopted for systematic microscopic studies of low- and high-energy spectroscopic properties. We will confine our review to low-energy spectroscopy. In vibrational nuclei, we will focus our attention on quadrupole collective modes and, especially, on the excitations described by states of mixed symmetry (ms) with respect to the exchange of proton–neutron pairs. These states were introduced within the IBM2. As we shall see, the QPM multiphonon states can be put in correspondence with the multiboson ones of the algebraic approach. This is not surprising since the IBM has to be viewed as a phenomenological realization of a fermion–boson mapping [35]. The mapping procedure was inspired by the boson expansion techniques developed in the 1960s [36–38]. The leading ideas of the fermion–boson mapping also underlie the QPM.

The correlation of the QPM with the IBM came out to be very fruitful. In most cases, the QPM provides the microscopic support to the IBM picture of some phenomena. On the other hand, it points out the role of the shell structure which is smoothed out in the algebraic approach. Moreover, it can be exploited to embed the RPA and QPM states within the IBM frame and, therefore, extend the microscopic analysis of low-lying collective modes to nuclei far away from proton and neutron shell closure, not directly accessible to the QPM. We will adopt this method to investigate magnetic and, especially, electric dipole collective excitations.

The QPM represents a precious tool for exploring the properties of well-deformed nuclei. It was widely adopted to investigate electric and magnetic collective excitations of several multipolarities [34]. It contributed considerably to clarify the nature of low-lying electric dipole modes [2].

Here, we will focus our attention on the 0^+ states which were produced in large abundance in several nuclei of the rare-earth and actinide regions [39–44].

2. A brief outline of the QPM

The QPM [34] adopts a Hamiltonian of the form

$$H = H_{\rm sp} + V_{\rm pair} + V_{\rm M}^{\rm ph} + V_{\rm SM}^{\rm ph} + V_{\rm M}^{\rm pp}. \tag{1}$$

$H_{\rm sp}$ is a one-body Hamiltonian which includes a Woods–Saxon potential $V_{\rm WS}$, $V_{\rm pair}$ is the monopole pairing, $V_{\rm M}^{\rm ph}$ and $V_{\rm SM}^{\rm ph}$ are, respectively, sums of separable multipole and spin–multipole interactions acting in the ph channel and $V_{\rm M}^{\rm pp}$ is the sum of particle–particle multipole

potentials. The ph separable pieces have the structure

$$V_{\rm M}^{\rm ph} = \sum_{\lambda\mu}^{\tau\tau'} \kappa_\lambda(\tau\tau') M^\dagger_{\lambda\mu}(\tau) M_{\lambda\mu}(\tau'), \tag{2}$$

$$V_{\sigma}^{\rm ph} = \sum_{\lambda\mu}^{\tau\tau'} \kappa_\lambda^{(\sigma)}(\tau\tau') S^\dagger_{\lambda\mu}(\tau) S_{\lambda\mu}(\tau'), \tag{3}$$

where $\tau = \pi, \nu$. The multipole pieces are

$$M_{\lambda\mu} = \sum_{qq'} \langle q|F_{\lambda\mu}|q'\rangle a^\dagger_q a_{q'}, \tag{4}$$

$$S_{\lambda\mu} = \sum_{qq'} \langle q|F^{(\sigma)}_{\lambda\mu}|q'\rangle a^\dagger_q a_{q'}, \tag{5}$$

where

$$F_{\lambda\mu} = R(r) Y_{\lambda\mu}(\hat{r}) = \frac{{\rm d}V_{\rm WS}}{{\rm d}r} Y_{\lambda\mu}(\hat{r}), \tag{6}$$

$$F^{(\sigma)}_{\lambda\mu} = R(r)[\sigma \otimes Y_{\lambda-1}(\hat{r})]_{\lambda\mu} = \frac{{\rm d}V_{\rm WS}}{{\rm d}r}[\sigma \otimes Y_{\lambda-1}(\hat{r})]_{\lambda\mu}. \tag{7}$$

The particle–particle potential acts among proton or neutron pairs only and has a similar structure

$$V_{\rm M}^{\rm pp}(\tau) = \sum_{\lambda\mu} G_\lambda(\tau) P^\dagger_{\lambda\mu}(\tau) P_{\lambda\mu}(\tau), \tag{8}$$

where

$$P^\dagger_{\lambda\mu} = \sum_{qq'} \langle q|R(r) Y_{\lambda\mu}(\hat{r})|q'\rangle a^\dagger_q a^\dagger_{q'}. \tag{9}$$

The QPM procedure goes through several steps. One first transforms the ph $a^\dagger_q$ (a_q) into qp $\alpha^\dagger_q$ (α_q) operators by making use of the Bogoliubov canonical transformation

$$\begin{aligned} a^\dagger_q &= u_q \alpha^\dagger_q + v_q \alpha_{\bar{q}} \\ a_q &= u_q \alpha_q + v_q \alpha^\dagger_{\bar{q}}, \end{aligned} \tag{10}$$

where $\alpha_{\bar{q}}$ and $\alpha^\dagger_{\bar{q}}$ are time-reversal operators. For a spherical basis, for instance, $\alpha_{\bar{q}} = (-)^{j-m}\alpha_{j-m}$.

The quasiparticle separable Hamiltonian so obtained is then adopted to generate the QRPA energies ω_λ and the corresponding phonons

$$Q^\dagger_\lambda = \frac{1}{2} \sum_{qq'} \left\{ \psi^\lambda_{qq'} \left[\alpha^\dagger_q \alpha^\dagger_{q'}\right]_\lambda - \varphi^\lambda_{qq'} [\alpha_{q'} \alpha_q]_{\bar{\lambda}} \right\}. \tag{11}$$

The $\psi^\lambda_{qq'}$ and $\varphi^\lambda_{qq'}$ amplitudes fulfill the equations

$$\frac{1}{2} \sum_{qq'} \left[\psi^\lambda_{qq'} \psi^{\lambda'}_{qq'} - \varphi^\lambda_{qq'} \varphi^{\lambda'}_{qq'} \right] = \delta_{\lambda\lambda'} \tag{12}$$

obtained from enforcing the normalization condition

$$\langle 0|Q_{\lambda'} Q^\dagger_\lambda|0\rangle = \langle 0|\left[Q_{\lambda'}, Q^\dagger_\lambda\right]|0\rangle \simeq \delta_{\lambda\lambda'} \tag{13}$$

valid in the quasiboson approximation.

Once the QRPA phonons are generated, it is possible to express the quasiparticle separable Hamiltonian into the phonon form

$$H_{\rm QPM} = \sum_{\lambda} \omega_{\lambda} Q^{\dagger}_{\lambda} Q_{\lambda} + H_{\rm vq}. \tag{14}$$

The first term is the unperturbed phonon Hamiltonian and $H_{\rm vq}$ is a PC piece whose exact expression can be found in [34].

The phonon Hamiltonian is diagonalized in a space spanned by states composed of one, two and three QRPA phonons yielding the eigenfunctions

$$\Psi_{\nu \rm JM} = \sum_{i} R^{(\nu J)}_{i} Q^{\dagger}_{i\rm JM}|0\rangle + \sum_{\lambda_1\lambda_2} P^{(\nu J)}_{\lambda_1\lambda_2}\big[Q^{\dagger}_{\lambda_1} \otimes Q^{\dagger}_{\lambda_2}\big]_{\rm JM}|0\rangle + \sum_{\lambda_1\lambda_2}^{\lambda_3 I} T^{(\nu J)}_{\lambda_1\lambda_2\lambda_3 I}\big[\big[Q^{\dagger}_{\lambda_1} \otimes Q^{\dagger}_{\lambda_2}\big]_{I} \otimes Q^{\dagger}_{\lambda_3}\big]_{\rm JM}|0\rangle, \tag{15}$$

where i and ν label, respectively, the QRPA phonons and the QPM states of a given spin JM.

The above wavefunctions are properly normalized and antisymmetrized according to the procedure outlined in [34, 45]. Use is made of the exact commutation relations [34, 46–48]

$$\big[Q_{\lambda}, Q^{\dagger}_{\lambda'}\big] = \frac{1}{2}\delta_{\lambda\lambda'} \sum_{qq'} \big[\psi^{\lambda}_{qq'}\psi^{\lambda}_{qq'} - \varphi^{\lambda}_{qq'}\varphi^{\lambda}_{qq'}\big] - \sum_{qq'} \mathcal{C}^{\lambda\lambda'}_{qq'} \alpha^{\dagger}_{q}\alpha_{q'}, \tag{16}$$

where

$$\mathcal{C}^{\lambda\lambda'}_{qq'} = \sum_{q_1} \psi^{\lambda}_{q'q_1}\psi^{\lambda'}_{qq_1} C^{\lambda}_{q'q_1} C^{\lambda'}_{qq_1} - \varphi^{\lambda}_{qq_1}\varphi^{\lambda'}_{q'q_1} C^{\bar{\lambda}}_{qq_1} C^{\bar{\lambda'}}_{q'q_1}.$$

While the first term corresponds to the boson approximation, the second one takes into account the internal fermion structure of phonons and insures the antisymmetrization of the multiphonon wavefunction (15). Such a term considerably affects the structure of the excited states in many spherical even–even nuclei [46–49].

Each one-body transition operator

$$\mathcal{M}(X\lambda) = \sum_{qq'} \langle q|M(X\lambda)|q'\rangle a^{\dagger}_{q} a_{q'}, \tag{17}$$

expressed in terms of quasiparticle and phonon operators, splits into two pieces [48]

$$M(X\lambda) = \mathcal{M}_{\rm ph}(X\lambda) + \mathcal{M}_{\rm sc}(X\lambda). \tag{18}$$

The first term is given by

$$\mathcal{M}_{\rm ph}(X\lambda\mu) = \frac{1}{2\hat{\lambda}} \sum_{qq'} \langle q\|M(X\lambda)\|q'\rangle (u_q v_{q'} \pm v_q u_{q'})\big(\psi^{\lambda}_{qq'} + \varphi^{\lambda}_{qq'}\big)\big(Q^{\dagger}_{\lambda} + Q_{\bar{\lambda}}\big), \tag{19}$$

where $\hat{\lambda} = \sqrt{2\lambda + 1}$ and the $+$ $(-)$ sign holds for time even (odd) operators. Being linear in the QRPA phonon operators Q_{λ} and $Q^{\dagger}_{\lambda}$, it connects states differing by one phonon. This is the leading term and promotes the *boson-allowed* transitions.

The second piece is a quasiparticle scattering term and is given by

$$\mathcal{M}_{\rm sc}(X\lambda) = \frac{1}{\hat{\lambda}} \sum_{qq'} \langle q\|M(X\lambda)\|q'\rangle (u_q u_{q'} \mp u_q u_{q'})[\alpha^{\dagger}_{q} \times \alpha_{q'}]_{\lambda}, \tag{20}$$

where the $-$ $(+)$ sign holds for time even (odd) operators. It links states with the same number of phonons, or differing by two phonons, and promotes the *boson-forbidden* transitions.

The first term is dominant in transitions between ground and one-phonon states. The second is responsible for the transitions between one-phonon states, which would be forbidden otherwise.

Table 1. Parameters of the Woods–Saxon potential in two typical nuclear regions.

Nucleus		r_0 (fm)	V_0 (MeV)	κ (fm^2)	α (fm^{-1})
^{136}Ba	N	1.28	43.40	0.413	1.613
	Z	1.31	53.43	0.349	1.538
^{94}Mo	N	1.29	44.70	0.413	1.613
	Z	1.24	56.86	0.338	1.587

One of the problems to be faced in the QPM is the determination of the Hamiltonian parameters. The Woods–Saxon parameters appropriate for the two regions around $N = 50$ and $N = 82$ are shown in table 1. They were determined in [50, 51] and yield single-particle spectra in overall agreement with the data [52]. The single-particle space includes all shells below the Fermi energy and all bound states above, so as to allow the investigation of the properties of the excited states over a wide energy range. A constant monopole pairing potential is used. Its value is obtained by a fit of odd–even mass differences. The coupling strength parameters κ_2 and κ_3 of the quadrupole–quadrupole and octupole–octupole ph potential are fixed by a fit to the energies of the first 2^+ and 3^- states. The strengths κ_λ of the other multipole terms are adjusted so as to leave unchanged the energy of the computed lowest two-quasiparticle states [52].

The multipole pairing interaction has been the object of thorough investigations since the first study of Belyaev [53]. It was shown [53, 54] to be necessary to restore the Galilean invariance. This request fixes the strength of the quadrupole pairing [54].

The quadrupole pairing turned out to be the only particle–particle potential relevant to low-energy spectra. It is assumed to be equal for protons and neutrons, $G_2 = G_2(\nu) = G_2(\pi)$ ($G_2(\nu\pi) = 0$). As we shall see, the quadrupole pairing plays a crucial role in determining the properties of the low-energy quadrupole modes.

The parameters in different mass regions were determined by procedures discussed in [46–49]. A unique set of parameters is used throughout the nuclei of a given mass region to calculate the low-lying as well as high-lying spectra.

Another problem is connected with the quasiparticle formalism and the quasiboson approximation underlying the QRPA. The Bogoliubov transformation (10) only conserves the particle number on average. The violation of the particle number is small. For example, in ^{136}Ba the violation of the neutron number is 6.5% of the valence neutrons and 2.5% of the total number of neutrons.

The validity of the quasiboson approximation can be tested by analyzing the influence of the ground-state correlations on the excited states within the RPA [8, 55–59] and QPM [60]. The effect is small for nuclei around closed shells, where the collectivity of the low-lying vibrational states is not too strong. In fact, the backward amplitudes $\varphi^\lambda_{qq'}$ entering the corresponding RPA phonons (11) are small. They are quenched by the strong quadrupole–pairing interaction. In the case of ^{136}Ba, only few components of the $\left[2^+_{is}\right]_{\mathrm{RPA}}$ have appreciable backward amplitudes.

In order to quantify the effect of the ground-state correlations, we have computed the ratio $\left(\varphi^\lambda_{qq'}\right)^2 / \left(\psi^\lambda_{qq'}\right)^2$. This turned out to be $\left(\varphi^\lambda_{qq'}\right)^2 / \left(\psi^\lambda_{qq'}\right)^2 \sim 0.06$, at most, for the neutron components and $\left(\varphi^\lambda_{qq'}\right)^2 / \left(\psi^{i\lambda}_{qq'}\right)^2 \sim 0.03$ for protons.

The backward amplitudes of the isovector $\left[2^+_{iv}\right]_{\mathrm{RPA}}$ are much smaller. We can then conclude that the contribution of the terms including backward amplitudes $\varphi^\lambda_{qq'}$ can be neglected except when $\varphi^\lambda_{qq'}$ is the leading term. This is the case of the direct excitation of the two-phonon states from the ground state [46–49].

Finally, we have to select the phonons to be included in the multiphonon basis used for diagonalizing the Hamiltonian (1). The choice of the phonon basis is dictated by the properties of the states to be determined. For low-lying positive parity QPM states, we include only phonons of positive parity. We consider phonons of multipolarities $\lambda = 1$–6 and, for each λ, we include all phonons up to a given energy. Since the QPM Hamiltonian mixes the multiphonon components differing by one phonon, the fragmentation of the two-phonon states is sensitive to the number of one- and three-phonon configurations. In the present calculation the one-phonon space was spanned by several RPA states of energy up to 5 MeV. Only in the case of 1^+ states, the one-phonon space was extended to an energy which includes the M1 resonance.

The structure of the QPM states changes as we increase the number of two-phonon basis states until this number reaches a saturation value. Increasing the number of two-phonon states further will not affect any longer the structure of the wavefunction (15). The onset of this plateau determines the dimensions of the multiphonon space to be used in actual calculations.

3. Symmetric and mixed-symmetry states in the IBM2

In the IBM2 the low-lying states are classified according to the number of their constituent s ($L = 0$) and d ($L = 2$) bosons and their symmetry with respect to the exchange of proton versus neutron bosons. The symmetry is determined by the F-spin quantum number [61], the boson counterpart of isospin. Proton and neutron bosons form an F-spin doublet with $F_3 = 1/2$ for protons and $F_3 = -1/2$ for neutrons. States with maximum F-spin, $F = F_{\max}$, are completely symmetric with respect to $\pi - \nu$ exchange. The other states with $F < F_{\max}$ have mixed symmetry. Only ms states with $F = F_{\max} - 1$ have been observed so far.

A clear picture of the structure of the IBM2 states is gained in the so-called Q-phonon scheme [62–64]. Such a scheme yields simple expressions containing only one or two Q-phonon configurations capable of describing the yrast, second 2^+ and second 0^+ states. It also yields different relations between transition matrix elements.

In the Q-phonon formalism, the states are given by the schematic formulas

$$\left|2_{\rm s}^+\right\rangle \propto Q_{\rm s}\left|0_1^+\right\rangle, \tag{21}$$

$$|2_{\rm ms}^+\rangle \propto Q_{\rm ms}|0_1^+\rangle, \tag{22}$$

$$|J_{\rm s}^+\rangle \propto [Q_{\rm s} \times Q_{\rm s}]^J|0_1^+\rangle, \tag{23}$$

$$|J_{\rm ms}^+\rangle \propto [Q_{\rm ms} \times Q_{\rm s}]^J|0_1^+\rangle, \tag{24}$$

where $|0_1^+\rangle$ is a correlated ground state and

$$Q_{\rm s} = Q_\pi + Q_\nu, \qquad Q_{\rm ms} = Q_\pi - Q_\nu \tag{25}$$

are, respectively, the $\pi - \nu$ symmetric (F-scalar) and antisymmetric (F-vector) components of the boson quadrupole operator.

The IBM $E2$ operator is composed of a sum of F-scalar and F-vector components

$$T(E2) = e_\pi Q_\pi + e_\nu Q_\nu = e_{\rm s}Q_{\rm s} + e_{\rm ms}Q_{\rm ms}, \tag{26}$$

where $Q_{\rm s}$ and $Q_{\rm ms}$ are given by (25) and the charges are $e_{\rm s} = (e_\pi + e_\nu)/2$ and $e_{\rm ms} = (e_\pi - e_\nu)/2$. The $M1$ operator has a similar structure

$$T(M1) = g_\pi L_\pi + g_\nu L_\nu = g_{\rm s}L_{\rm s} + g_{\rm ms}L_{\rm ms}, \tag{27}$$

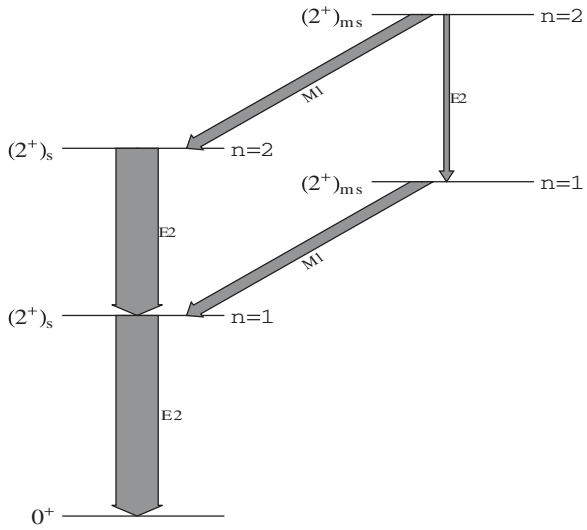

Figure 1. Signature of symmetric and mixed-symmetry states.

where

$$L_s = L_\pi + L_\nu, \qquad L_{ms} = L_\pi - L_\nu. \tag{28}$$

The corresponding gyromagnetic ratios are $g_s = (g_\pi + g_\nu)/2$ and $g_{ms} = (g_\pi - g_\nu)/2$.

Both components of the $E2$ operator couple states that differ by one d boson. On the other hand, the F-scalar $E2$ operator connects states of the same $\pi - \nu$ symmetry, while the F-vector component couples ms to symmetric states differing by one d boson.

The F-scalar $M1$ operator, being proportional to the total angular momentum, does not promote any transition. The F-vector component, instead, connects ms with symmetric states, both having the same number of d bosons. Its main action, in fact, is to transform an F-scalar into an F-vector quadrupole boson

$$\begin{aligned} L_{ms}|2_s^+\rangle &= L_{ms}Q_s|0_1^+\rangle = (L_\pi - L_\nu)(Q_\pi + Q_\nu)|0_1^+\rangle \\ &= (L_\pi Q_\pi - L_\nu Q_\nu)|0_1^+\rangle \propto (Q_\pi - Q_\nu)|0_1^+\rangle. \end{aligned} \tag{29}$$

This formula points out that the one-phonon ms state describes a $\pi - \nu$ scissors-like oscillation mode built on an excited quadrupole vibrational mode.

It is also clear from the above description that the $E2$ and $M1$ transition strengths provide the signature of the low-lying states in vibrational nuclei, as illustrated schematically in figure 1.

It is possible to state a correspondence of the IBM with the QPM states. The d bosons correspond to the quadrupole QRPA phonons $Q^\dagger_{\lambda=2}$. This is not surprising. In fact, the IBM states result from a boson mapping of highly correlated fermion pairs. Correspondingly, the RPA phonons are composed of correlated quasiparticle pairs. The isospin nature of the QRPA phonons can be deduced from the phase relations between the proton and neutron quasiparticle pair components. More quantitative, it can be determined by computing the ratio [65]

$$R_Q(2^+) = \frac{|\langle 2^+_{RPA}|Q_{iv}|0^+_{RPA}\rangle|^2}{|\langle 2^+_{RPA}|Q_{is}|0^+_{RPA}\rangle|^2}, \tag{30}$$

where

$$Q_{is} = Q^{(p)} + Q^{(n)}, \qquad Q_{iv} = Q^{(p)} - Q^{(n)} \tag{31}$$

are the isoscalar and isovector fermion quadrupole operators expressed in terms of the proton and neutron operators

$$Q_{\mu}^{(\tau)} = \sum_{i}^{\tau} r_i^2 Y_{2\mu}(\hat{r}_i). \tag{32}$$

The $\left|2^+_{\mathrm{RPA}}\right\rangle$ state can be considered isoscalar or isovector according that $R_Q(2^+) < 1$ or $R_Q(2^+) > 1$, respectively.

4. Low-lying collective modes: experimental evidence and theoretical description

The most prominent low-lying collective modes have an isoscalar or symmetric character. The lowest 2^+_1, for instance, which describes a quadrupole surface vibration of protons and neutrons in phase, is present in all spherical or weakly deformed nuclei and carries a large $E2$ strength. The corresponding isoscalar quadrupole modes in deformed nuclei are known as β and γ vibrational states.

The mixed-symmetry states eluded experimental observation for long time. The first collective excitation of this nature was observed in deformed nuclei and is known as scissors mode. This was predicted in a geometrical model [66] and discovered by Richter and co-workers in an (e, e') experiment [67]. It is a $J^\pi = 1^+$ mode at an excitation of about 3 MeV and is strongly excited from the ground state with a large $M1$ strength. Its discovery has triggered a long series of experimental and theoretical investigations that have ascertained its existence in most deformed nuclei. These systematic studies have also provided a complete characterization of the mode. Its many facets were discussed in several review papers [2, 68–70].

The lowest ms state in spherical and weakly deformed nuclei has $J^\pi = 2^+$ and, therefore, cannot be excited directly from the ground state through an $M1$ transition, hence the difficulty of detecting such a mode. Its first evidence was inferred from the analysis of the $E2/M1$ mixing and branching ratios in $N = 84$ isotones [71]. Several subsequent works have guessed the mixed-symmetry character of low-spin states in vibrational and transitional nuclei on the ground of similar arguments [72–76] or by exploiting the sensitivity of the probe to isospin [77–80]. A more reliable assessment of the mixed-symmetry nature of 2^+ states could be made after the measurements of absolute electromagnetic decay strengths [81–89].

A conclusive evidence was provided by an experiment on ^{94}Mo exploiting β-decay as a populating mechanism [90]. This and other subsequent experiments using different techniques [91–93] have produced an impressive body of data which greatly enriched our knowledge about the low-energy spectrum of this nucleus.

Since then, a series of experiments has systematically discovered and studied low-energy modes in several other nuclei in the proximity of $N = 50$ [94–101] and $N = 82$ [102–110].

In all the above experiments, the analysis of the data was carried out within the framework of the IBM2. This, indeed, is a natural tool for classifying the states according to the $\pi - \nu$ symmetry and the number of constituent bosons. IBM2 is also ideal for systematics throughout the periodic table.

These experimental discoveries have also triggered several microscopic studies. Some of them were carried out in a restricted shell model space [96, 97, 100]. More recently, large-scale shell model calculations using realistic two-body potentials were performed to study the structure of ms states in $N = 80$ isotones [111–113]. Shell model calculations are exact in principle and include a large number of configurations. These, however, are all low-lying $0 - \hbar\omega$ configurations. High-energy configurations are included in the QPM. Because of its flexibility, the QPM lends itself to systematic studies of low-energy spectra. In fact, this

Table 2. QRPA isoscalar to isovector $E2$ ratio and transition strengths versus the ratio G_2/κ_2 in ^{136}Ba (taken from [45]).

G_2/κ_2	$R_Q(2^+)$	$B(E2; g.s. \to 2^+_{iv})_{\rm RPA}$	$B(M1; 2^+_{iv} \to 2^+_{is})_{\rm RPA}$
		$[e^2b^2]$	$[\mu_N^2]$
0	0.58	0.0032	0.042
0.85	22.6	0.011	0.24

Table 3. Quasiparticle composition of the lowest 2^+ RPA phonons in ^{136}Ba and the corresponding $E2$ strength and isovector to isoscalar $R_Q(2^+)$ ratios (taken from [45]).

	ω (MeV)	Structure	$B(E2)\uparrow$ $[e^2b^2]$	$R_Q(2^+)$
2^+_{is}	0.95	$0.76(1h_{11/2})^2_n + 0.72(2g_{7/2})^2_p$ $0.24(3s_{1/2}2d_{3/2})_n + 0.43(2d_{5/2})^2_p$ $0.31(2d_{3/2})^2_n + 0.23(1g_{7/2}2d_{3/2})_p$	0.51	0.0034
2^+_{iv}	2.009	$0.85(1h_{11/2})^2_n - 0.98(1g_{7/2})^2_p$ $0.37(2d_{3/2})^2_n - 0.17(2d_{5/2})^2_p$ $0.22(3s_{1/2}2d_{3/2})_n - 0.1(1h_{11/2})^2_p$	0.011	22.6

approach has allowed systematic theoretical studies of ms states in nuclei around $N = 50$ [45, 114–116] and near $N = 82$ [117, 118] to be performed.

4.1. QRPA quadrupole states

The occurrence of an isovector QRPA 2^+ state at low energy is the preliminary condition for obtaining the QPM counterparts of the IBM ms states. In QRPA, the $\pi - \nu$ symmetry of the low-lying 2^+ states is tested by computing the ratio $R_Q(2^+)$ defined by (30). This ratio shows that, in all nuclei, the first $[2^+]_{\rm RPA}$ state is an isoscalar, or $\pi - \nu$ symmetric, mode. It will be denoted by $\left[2^+_{is}\right]_{\rm RPA}$. Its properties are determined almost solely by the isoscalar quadrupole–quadrupole interaction.

The occurrence of an isovector low-lying $[2^+]_{\rm RPA}$ state depends critically on the competition between quadrupole–quadrupole and quadrupole–pairing forces. The example of ^{136}Ba shown in table 2 is illustrative of all nuclei. The dramatic increase of the $R_Q(2^+)$ ratio with G_2/κ_2 indicates clearly that the second $[2^+]_{\rm RPA}$ changes from isoscalar to isovector.

Thus, in order to have a low-lying mixed-symmetry 2^+ state, it is necessary to choose comparable quadrupole–pairing and quadrupole–quadrupole strengths, $G_2 \sim \kappa_2$. We will denote this RPA state as $\left[2^+_{iv}\right]_{\rm RPA}$. Its collectivity increases as G_2/κ_2 increases. Indeed, both $B\big(E2; 0^+_{\rm gs} \to \left[2^+_{iv}\right]_{\rm RPA}\big)$ and $B\big(M1; \left[2^+_{iv}\right]_{\rm RPA} \to \left[2^+_{is}\right]_{\rm RPA}\big)$ strengths grow with G_2/κ_2.

The isospin nature of the $[2^+]_{\rm RPA}$ states can be tested also by looking at the phase relations between the neutron and proton components of the RPA phonons (11). As shown in table 3 for ^{136}Ba, the proton and neutron forward amplitudes ψ are in phase in the $\left[2^+_{is}\right]_{\rm RPA}$ and in opposition of phase in the $\left[2^+_{iv}\right]_{\rm RPA}$. For an appropriate value of the ratio G_2/κ_2 (=0.8–0.9), which is close to the estimations made in [54], the RPA basis contains a collective isoscalar $\left[2^+_{is}\right]_{\rm RPA}$ and a slightly collective isovector $\left[2^+_{iv}\right]_{\rm RPA}$ state. The two states are mutually coupled via a strong M1 transition.

Table 4. Energy and phonon structure of selected low-lying excited states in ^{94}Mo and ^{136}Ba. Symmetric and non-symmetric states are denoted by |s⟩ and |ms⟩, respectively. The data are taken from [45].

^{A}X		J^{π}	E (MeV)		Structure,%
			EXP	QPM	
^{94}Mo		2_1^+	0.871	0.860	$93\%[2_{is}^+]_{\mathrm{RPA}}$
	|s⟩	2_2^+	1.864	1.750	$82\%[2_{is}^+ \otimes 2_{is}^+]_{\mathrm{RPA}}$
		4_1^+	1.573	1.733	$82\%[2_{is}^+ \otimes 2_{is}^+]_{\mathrm{RPA}}$
		2_3^+	2.067	1.940	$95\%[2_{iv}^+]_{\mathrm{RPA}}$
		2_4^+	2.393	2.730	$27\%[2_{is}^+ \otimes 2_{iv}^+]_{\mathrm{RPA}}$
	|ms⟩	2_5^+	2.870	3.014	$59\%[2_{is}^+ \otimes 2_{iv}^+]_{\mathrm{RPA}}$
		3_2^+	2.965	2.940	$87\%[2_{is}^+ \otimes 2_{iv}^+]_{\mathrm{RPA}}$
		1_2^+	3.129	2.880	$90\%[2_{is}^+ \otimes 2_{iv}^+]_{\mathrm{RPA}}$
	|spin − flip⟩	1_3^+	3.512	3.550	$40\%[1^+]_{\mathrm{RPA}}$
^{136}Ba		2_1^+	0.810	0.760	$77\%[2_{is}^+]_{\mathrm{RPA}} + 19\%[2_{is}^+ \otimes 2_{is}^+]_{\mathrm{RPA}}$
	|s⟩	2_2^+	1.551	1.640	$48\%[2_{is}^+ \otimes 2_{is}^+]_{\mathrm{RPA}} + 17\%[2_{is}^+]_{\mathrm{RPA}}$
		4_1^+	1.866	1.630	$60\%[2_1^+ \otimes 2_1^+]_{\mathrm{RPA}}$
		2_4^+	2.129	1.850	$73\%[2_{iv}^+]_{\mathrm{RPA}}$
		1_2^+	2.694	2.800	$85\%[2_{is}^+ \otimes 2_{iv}^+]_{\mathrm{RPA}}$
	|ms⟩	2_5^+		3.120	$51\%[2_{is}^+ \otimes 2_{iv}^+]_{\mathrm{RPA}}$
		4_2^+		3.230	$41\%[2_{is}^+ \otimes 2_{iv}^+]_{\mathrm{RPA}}$
		3_2^+		3.040	$90\%[2_{is}^+ \otimes 2_{iv}^+]_{\mathrm{RPA}}$
	|noncoll⟩	2_3^+	2.080	2.370	$\sim \|q_1 q_2\rangle$

4.2. QPM multiphonon states and transitions

Once at least one isoscalar and one isovector QRPA quadrupole excitation mode have been ascertained to occur at low energy, it is possible to face the final task, namely to generate within the QPM the microscopic states and investigate their $\pi - \nu$ symmetry and phonon composition.

As shown in table 4, most of the QPM states in ^{94}Mo have a dominant component which exhausts 60% –90% of the norm of the total wavefunction. The table also shows that in ^{136}Ba most of the states are fragmented. In fact, several one- and two-phonon components get admixed. Analogous structure is observed for the states of the other nuclei in the vicinity of $N = 82$.

Going into the details, we observe that the lowest isoscalar and isovector 2^+ states have a dominant one-phonon component. The others are mainly two-phonon states with a dominant symmetric $\left[2_{is}^+ \otimes 2_{is}^+\right]_{\mathrm{RPA}}$ or mixed-symmetry $\left[2_{is}^+ \otimes 2_{iv}^+\right]_{\mathrm{RPA}}$ component. There are also non-collective states which do not fall in either of the two groups. The 2_3^+ shown in table 4 is an example.

The phonon structure of the states combined with the isospin properties of the phonons leads to well-defined $E2$ and $M1$ selection rules. As shown in table 5, only the $E2$ transitions among states differing by one phonon are strong. They are promoted by the phonon–exchange term (19) of the transition operator. The $E2$ operator promotes mainly transitions between states of the same $\pi - \nu$ symmetry. Especially enhanced are the $E2$ transitions between $\pi - \nu$ symmetric states. Weak $E2$ transitions occur between symmetric and ms states, only if they differ by an even number of phonons. They are promoted by the scattering term (20).

A reverse pattern holds for the $M1$ transitions (table 6). These occur only between states with an equal number of phonons or differing by two phonons, like in the $1_2^+ \to 0_1^+$ transition.

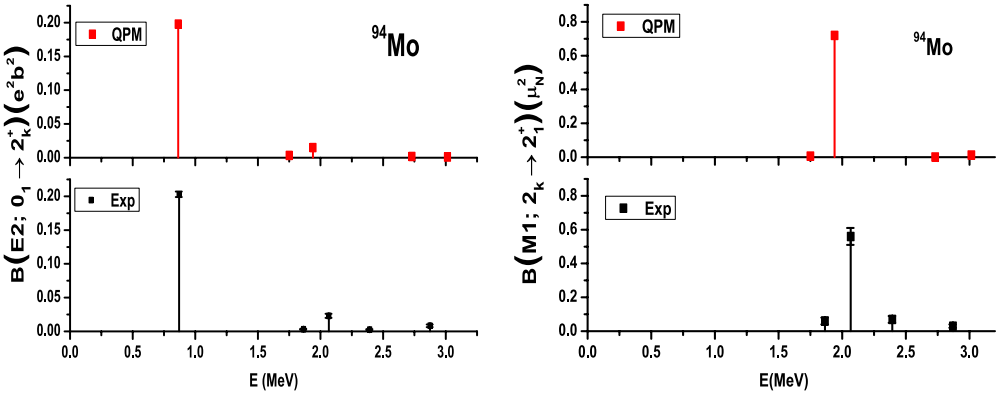

Figure 2. $B(E2; 0_1^+ \rightarrow 2_k^+)$ and $B(M1; 2_k^+ \rightarrow 2_1^+)$ strength distributions in ^{94}Mo.

Table 5. $B(E2)(e^2b^2)$ strengths in ^{94}Mo. Δn_{ph} gives the difference in the number of phonons between initial and final states. The theoretical values are from [45]. The experimental data are taken from [90, 91, 93].

		Δn_{ph}	$J_i \rightarrow J_f$	Exp	QPM	IBM2
	$\|s\rangle \rightarrow \|s\rangle$	1	$0_1^+ \rightarrow 2_1^+$	0.2030(40)	0.1978	0.2333
		1	$2_2^+ \rightarrow 2_1^+$	0.0720(260)	0.0673	0.0592
IS		1	$4_1^+ \rightarrow 2_1^+$	0.0670(100)	0.0661	0.0592
		2	$0_1^+ \rightarrow 2_2^+$	0.0032(7)	0.035	0
	$\|ms\rangle \rightarrow \|ms\rangle$	1	$1_2^+ \rightarrow 2_3^+$	<0.0690	0.0374	0.0556
		1	$0_1^+ \rightarrow 2_3^+$	0.0230(30)	0.0150	0.0151
		1	$1_2^+ \rightarrow 2_1^+$	0.0030(10)	0.0013	0.0049
IV		2	$0_1^+ \rightarrow 2_4^+$	0.0027(8)	0.018	0
		2	$0_1^+ \rightarrow 2_5^+$	0.0083(10)	0.010	0

Table 6. $B(M1)(\mu^2)$ strengths in ^{94}Mo. The theoretical values are from [45]. The experimental data are taken from [90, 91, 93].

Δn_{ph}	$J_i \rightarrow J_f$	Exp	QPM	IBM2
0	$2_3^+ \rightarrow 2_1^+$	0.56(5)	0.72	0.30
0	$2_5^+ \rightarrow 2_2^+$	0.27(3)	0.24	0.1
0	$1_2^+ \rightarrow 2_2^+$	0.44(3)	0.75	36
0	$3_2^+ \rightarrow 2_2^+$	0.24(3)	0.34	0.18
0	$3_2^+ \rightarrow 4_1^+$	0.075(10)	0.26	0.18
2	$1_2^+ \rightarrow 0_1^+$	$0.160^{+0.011}_{-0.010}$	0.14	0.16
1	$2_5^+ \rightarrow 2_1^+$	$0.0017^{+0.0010}_{-0.0012}$	0.001	0
1	$1_2^+ \rightarrow 2_1^+$	0.012(3)	0.0006	0

The transitions between ms and symmetric states are enhanced while those linking states of the same $\pi - \nu$ symmetry are suppressed.

The transition pattern determined by the selection rules is pictorially illustrated in figures 2 and 3. The $\pi - \nu$ symmetric, mainly one-phonon, 2_1^+ state collects by far the largest $E2$ strength (left panel of figure 2), while the $M1$ strength goes mostly to the ms one-phonon 2_3^+ state (right panel of figure 2).

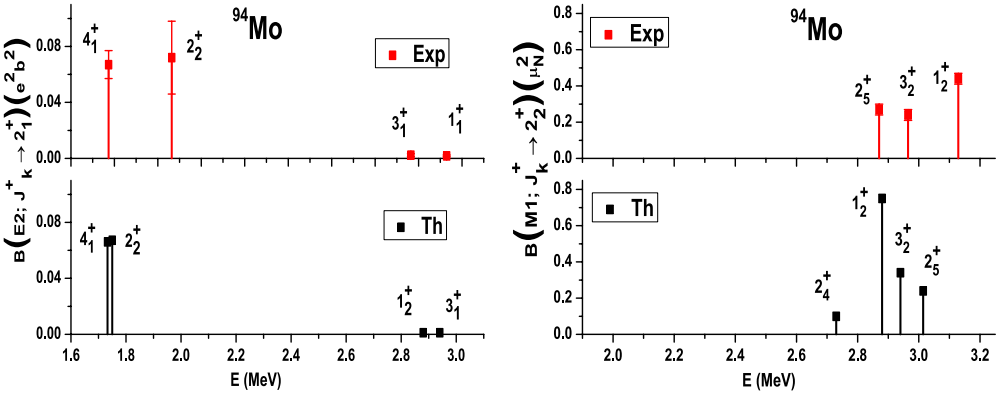

Figure 3. $E2$ and $M1$ strength distributions in ^{94}Mo.

The same rule applies to the multiphonon states. The $E2$ strength goes almost entirely to the symmetric, dominantly two-phonon, 2_2^+ and 4_1^+ states decaying to the one-phonon 2_1^+ of the same symmetry (left panel of figure 3).

The $M1$ strength goes mostly to the dominant two-phonon 1_2^+, 2_5^+ and 3_2^+ ms states decaying to the $\pi - \nu$ symmetric two-phonon 2_2^+ (right panel of figure 3). The 1_2^+, 2_5^+ and 3_2^+ states may be viewed as the components of a scissors multiplet built on the 2_2^+ state. Such a multiplet collects an $M1$ strength of the order $\sum_n B_n(M1) \sim 0.9$–$1\mu_N^2$.

Although differing in the details, the QPM energies and strengths are in overall good agreement with the experimental data. They are consistent with the IBM picture. The transitions allowed in the IBM2 are strong in the QPM. Those forbidden in IBM2 are weak in the QPM. This correspondence is almost one to one, with few exceptions.

In ^{94}Mo, for instance, the measured $1_2^+ \to 0_1^+$ and $1_3^+ \to 0_1^+$ $M1$ strengths are both reproduced by the QPM calculation. The 1_2^+ and 1_3^+ states, however, have a totally different structure. As shown in table 4, 1_2^+ is basically a two-phonon ms state, consistently with the IBM picture. In this algebraic approach the $M1$ transition of this ms state to the ground state is forbidden in the $U(5)$ spherical vibrational limit and is allowed only in the $O(6)$ limit. In the QPM the $1_2^+ \to 0_1^+$ transition is boson forbidden and is promoted by the scattering term of the $M1$ operator (20).

The other 1_3^+ state, instead, has a composite structure and contains a sizable $[1^+]_{\mathrm{RPA}}$ with the dominant spin–flip quasiparticle configuration $(2p_{3/2} \otimes 2p_{1/2})$. This component is responsible for the transition to the ground state. Such a transition is out of the domain of the algebraic IBM.

The role of the shell structure also emerges from a series of experiments in some $N = 80$ [104] and $N = 84$ [85, 88] isotones, where the $E2$ (figures 4 and 5) and $M1$ (figure 6) strengths are distributed over few 2^+ states. Especially fragmented is the strength of the $M1$ transitions in the $N = 84$ isotones (figure 6). In these isotones, the isovector RPA 2^+ state is almost degenerate with the symmetric quadrupole–quadrupole two-phonon states as a result of the gap between the j-subshells present in the neutron single-particle spectrum above the $N = 82$ closed shell. The PC is, therefore, especially effective.

The gap between j-subshells is absent in the neutron hole spectra of the $N = 80$ isotones, hence the lack of splitting in nuclei like ^{136}Ba [89] (figure 6). An appreciable fragmentation is present in ^{138}Ce, nonetheless. In this nucleus, the mechanism responsible for such a phenomenon is a different one. It is promoted by the gap in correspondence of the proton

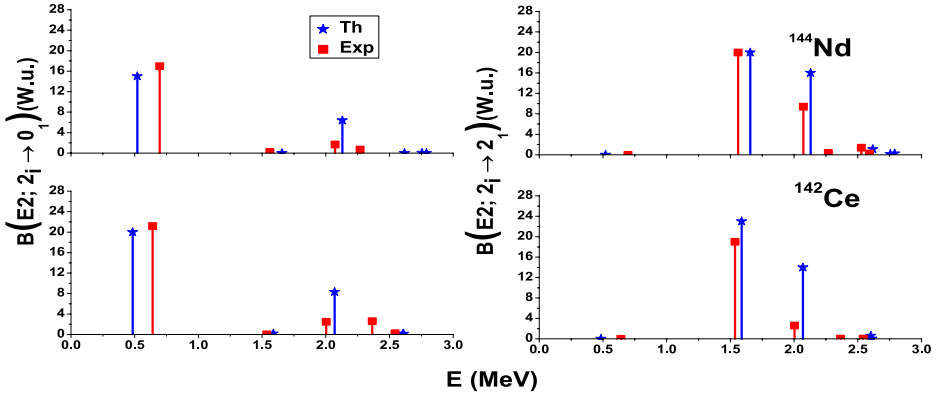

Figure 4. Distribution of the $2_i^+ \rightarrow 0_1^+$ (left) and $2_i^+ \rightarrow 2_1^+$ (right) $E2$ strengths in ^{142}Ce (bottom) and ^{144}Nd (top) (from [118]).

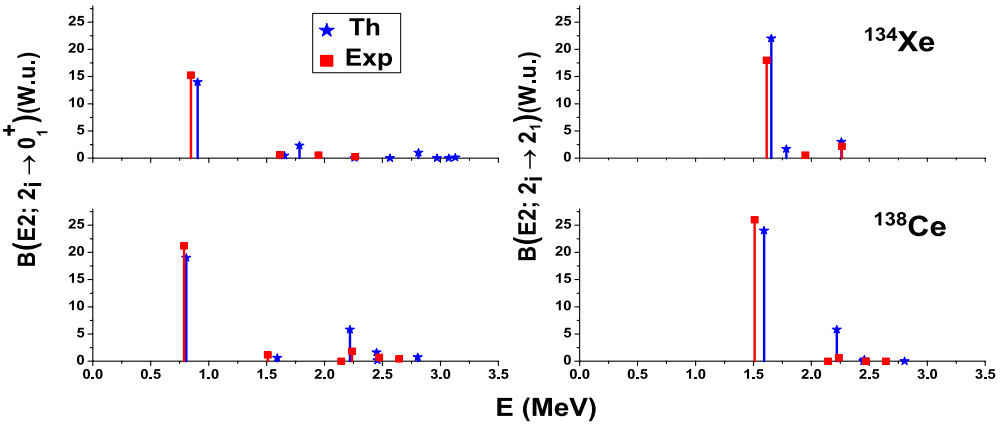

Figure 5. Distribution of the $2_i^+ \rightarrow 0_1^+$ (left) and $2_i^+ \rightarrow 2_1^+$ (right) $E2$ strengths in ^{138}Ce (bottom) and ^{134}Xe (top) (from [117]).

$1g_{7/2}$ subshell closure and the pairing responsible for the diffuseness of the Fermi surface which yields a relatively higher density of two-quasiparticle states at low energy. This leads to a higher number of low-lying states of mixed-symmetry character, hence the splitting of the M1 strength. Though different, both mixing mechanisms are genuine shell effects that can be explained only within a microscopic context which goes beyond the algebraic IBM and, even, the approaches like the QRPA based on the harmonic approximation.

4.3. Probing the mixed-symmetry states through electron and proton scattering

Scattering experiments using probes sensitive to isospin give information complementary to γ-ray spectroscopy. Early experiments of this kind consisted in combining inelastic proton and deuteron scattering [77–80]. The F-spin content could be related to changes in the cross-sectional ratio $\sigma(p, p')/\sigma(d, d')$.

A thorough test of the symmetry character and the phonon content of low-lying states was provided recently by a combined analysis of (e, e') and (p, p') experiments on ^{94}Mo [119, 120] and ^{92}Zr [120, 121], in which all low-lying 2^+ states get populated. The different

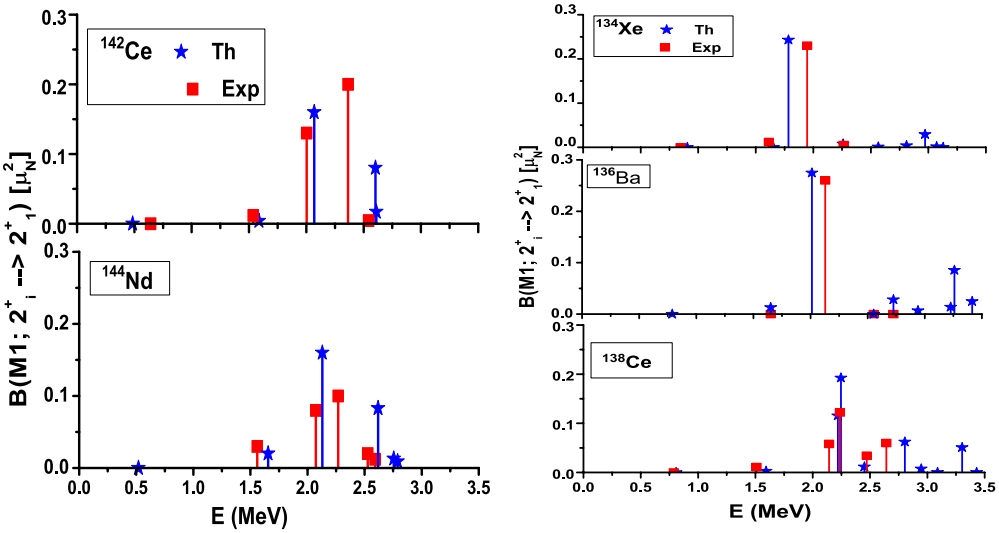

Figure 6. $M1$ strength distributions in $N = 84$ (left) and $N = 80$ (right) isotones, taken from [118] and [117], respectively.

sensitivity of the two probes to isospin allowed to establish the $\pi - \nu$ symmetry of each 2^+. In fact, electrons couple only to protons, while proton scattering is dominated by the isoscalar central part of the effective proton–nucleus interaction.

Let us consider the proton and neutron transition densities of the 2^+_s and 2^+_{ms} states in ^{92}Zr. The wavefunctions of these states are

$$|2^+_s\rangle = +0.85|(2d_{5/2})^2\rangle_n + 0.36|(1g_{9/2})^2\rangle_p + \ldots$$
$$|2^+_{ms}\rangle = -0.54|(2d_{5/2})^2\rangle_n + 0.57|(1g_{9/2})^2\rangle_p + \ldots, \quad (33)$$

where the dotted lines (. . .) stand for the remaining components contributing to the transitions. The phase relations confirm the isovector character of the second state.

The neutron (left-hand side) and proton (right-hand side) transition densities of the symmetric (top) and mixed-symmetry (bottom) 2^+ states just described are plotted in figure 7.

An out-of-phase coupling between the neutron valence–shell contribution and the contribution from the collective piece in the 2^+_{ms} state leads to a destructive quantum interference that reduces the neutron transition density at large radii (due to the larger radius of the $(2d_{5/2})^2_n$ orbital) and consequently shifts the maximum of the full neutron transition density to the interior with respect to that one of the 2^+_s state, as indicated by the arrows in the left-hand side of figure 7. This effect reduces the neutron transition radius of the 2^+_{ms} with respect to the 2^+_s. In contrast, the proton transition radius remains essentially unchanged since the $(1g_{9/2})^2_p$ components have the same sign in both states and, therefore, contribute constructively to the transition.

As already pointed out, two probes with different sensitivity to protons and neutrons are needed to study this quantum interference experimentally. Electron scattering at low momentum transfer provides a measure of the charge transition radius. Data covering a momentum-transfer range $q \simeq 0.3$–0.6 fm^{-1} [120, 121] were obtained from an (e, e') scattering experiment performed at the Darmstadt superconducting electron linear accelerator (S-DALINAC). They indicate no difference between the charge transition radii of the the 2^+_s and 2^+_{ms} states within experimental uncertainties (figure 7, top).

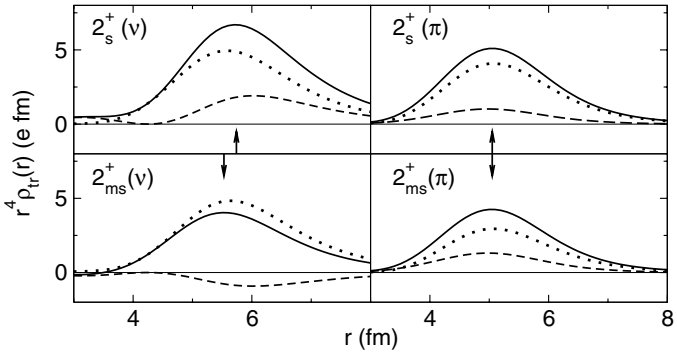

Figure 7. QPM neutron (left-hand side) and proton (right-hand side) transition densities of the 2^+_s (top) and 2^+_{ms} (bottom) states in ^{92}Zr (taken from [120]). The full transition densities (solid lines) are decomposed in parts stemming from the main two-quasiparticle configurations (dashed lines) and from all other configurations (dotted lines). The arrows indicate the maxima of the corresponding full transition densities.

Information about the neutron transition radii can be derived from the proton scattering data [122]. At an incident energy of 800 MeV, the protons interact predominantly via the isoscalar central piece of the effective projectile–nucleus interaction [123]. Clearly, the refraction patterns of the (p, p') cross section for the 2^+_{ms} state are shifted to higher q values as compared to those of the 2^+_s state (figure 7, bottom) corresponding to a smaller transition radius. The combination of both data sets unambiguously demonstrates that the phase of the neutron valence–shell configurations changes its sign between the 2^+_s and 2^+_{ms} states.

The transition densities from figure 7 were used to evaluate the cross sections in distorted wave Born approximation with the codes DWBA07 [124] for proton scattering and the one described in [125] for electron scattering. The T-matrix parametrization of Franey and Love [123] was used to describe the effective proton–nucleus interaction. The QPM calculation reproduces well both the absolute values of cross sections for both probes and the shift of the refraction pattern to higher q values for the 2^+_{ms} state in the (p, p') reaction as displayed in figure 8. The same effect is detected in ^{94}Mo [119, 120].

4.4. Mixed-symmetry states away from shell closure

The above analysis was limited to nearly spherical nuclei. It is, on the other hand, of great interest to study the evolution of ms states along a path which goes from vibrational to deformed nuclei and see, for instance, if they disappear at some critical point when permanent deformation sets in and the scissors mode appears.

Xe isotopes offer an almost unique opportunity to carry out such a study. A series of experiments has provided a large abundance of data on the isotopic chain $^{124-134}$Xe [87, 102, 107–110, 126].

The evolution of these states from the vibrational regime to deformation was studied within the algebraic IBM. Shell model approaches could just face the study of the isotopes in the proximity of the neutron shell closure [113].

The QPM is not suited to such a study. Being based on the quasiboson approximation, the QPM relies on the assumption that the ground-state correlations are not very pronounced. This is not the case of the nuclei in which both protons and neutrons are away from shell closures.

On the other hand, the correspondence between QPM and IBM suggests a way of disclosing, partly, the microscopic structure of low-lying states even in nuclei of the transitional region. This way consists in mapping the RPA phonon operators into the IBM bosons [127].

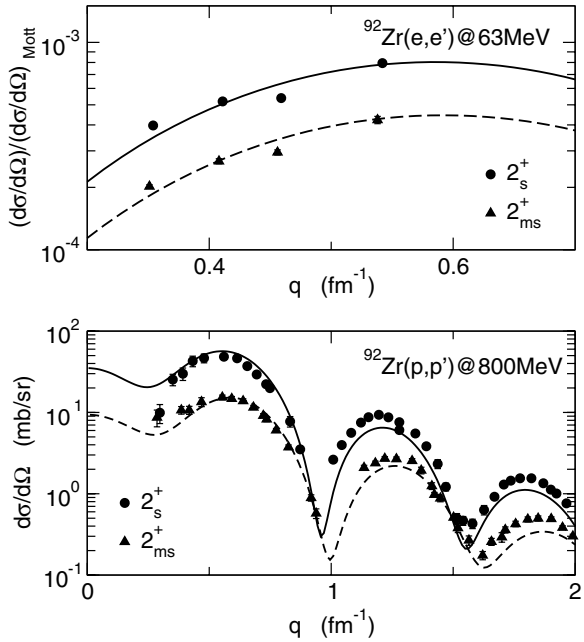

Figure 8. Momentum-transfer dependence of the experimental and QPM cross sections of the 2^+_s and 2^+_{ms} in electron (top) and proton (bottom) scattering (taken from [120]).

We consider the Hamiltonian

$$H = H_{\rm ms} + H_{\rm coll}. \tag{34}$$

Here, $H_{\rm ms}$ is the mixed-symmetry Hamiltonian, assumed to be harmonic in the RPA phonon operators $(b_{\rm ms}, b^\dagger_{\rm ms})$

$$H_{\rm ms} = \epsilon_{\rm ms} b^\dagger_{\rm ms} \cdot b_{\rm ms}, \tag{35}$$

where $\epsilon_{\rm ms}$ is the energy of the RPA phonons. The other term is obtained by the mapping of the RPA phonons into IBM bosons. Let us consider the quasiparticle quadrupole–quadrupole Hamiltonian

$$H = \sum_{\rm s} \epsilon_{\rm s} \alpha^\dagger \alpha_{\rm s} - \kappa Q^\dagger \cdot Q. \tag{36}$$

We express the quadrupole operator in terms of the RPA isoscalar quadrupole phonon operators $(b^\dagger, b)$. Keeping only the most collective phonons, we obtain

$$H_{\rm coll} = \omega_1 \left[\frac{5}{2} + b^\dagger \cdot b\right] + \omega_2 [b^\dagger \cdot b^\dagger + h.c], \tag{37}$$

where

$$\omega_1 = \sum_{\rm rs} \epsilon_{\rm rs} \left[\left(\psi^{(1)}_{\rm rs}\right)^2 + \left(\varphi^{(1)}_{\rm rs}\right)^2\right] - \frac{1}{\sqrt{5}}\kappa \left[\sum_{\rm rs} Q^{\rm (qp)}_{\rm rs} \left(\psi^{(1)}_{\rm rs} + \varphi^{(1)}_{\rm rs}\right)\right]^2 \tag{38}$$

$$\omega_2 = \sum_{\rm rs} (\epsilon_{\rm rs}) \left(\psi^{(1)}_{\rm rs}\right) \varphi^{(1)}_{\rm rs} - \frac{1}{2\sqrt{5}}\kappa \left[\sum_{\rm rs} Q^{\rm (qp)}_{\rm rs} \left(\psi^{(1)}_{\rm rs} + \varphi^{(1)}_{\rm rs}\right)\right]^2. \tag{39}$$

We have put $\epsilon_{\rm rs} = (\epsilon_{\rm r} + \epsilon_{\rm s})/2$ and $Q^{\rm (qp)}_{\rm rs} = Q_{\rm rs}(u_{\rm r} v_{\rm s} + u_{\rm s} v_{\rm r})$.

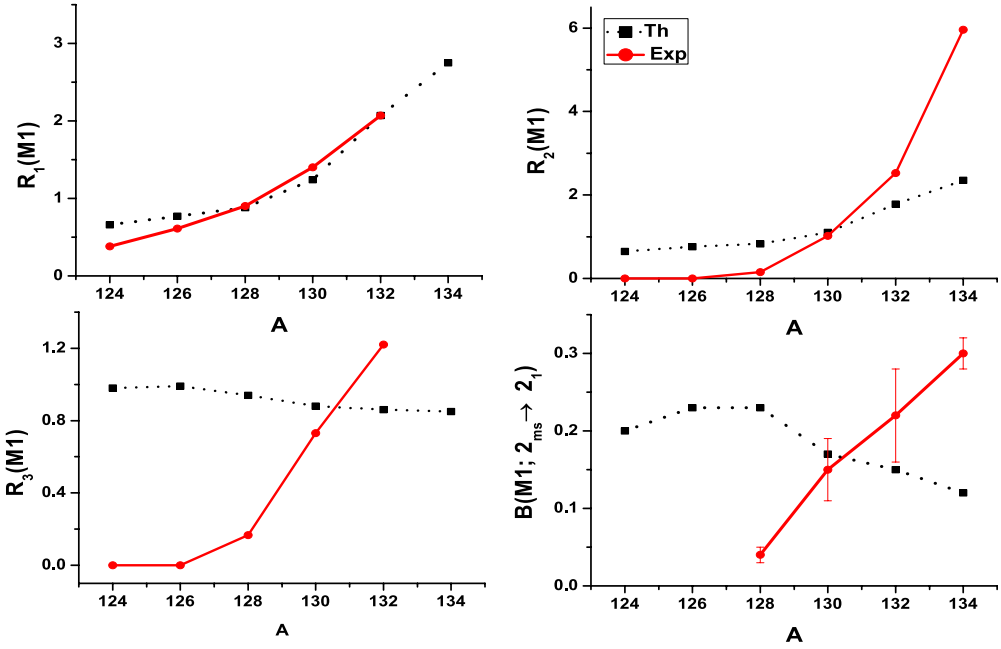

Figure 9. Trend of $M1$ reduced strengths and $M1$ ratios in the chain of Xe isotopes. The data are taken from [127].

The Hamiltonian (37) can be turned into an IBM Hamiltonian by replacing the RPA phonons with the IBM d bosons ($b \to d$) and introducing the s boson so that the number of bosons is conserved. After adding the ms piece (35), we obtain

$$H_{\rm coll} = \epsilon_{\rm ms} b^{\dagger}_{\rm ms} \cdot b_{\rm ms} + \omega_1 \left[\frac{5}{2} + d^{\dagger} \cdot d\right] + \omega_2 \frac{1}{N(N-1)} [b^{\dagger} \cdot b^{\dagger} {\rm ss} + {\rm h.c.}]. \tag{40}$$

We have now an IBM Hamiltonian whose parameters can be computed microscopically. A similar mapping procedure is applied to the scissors component of the $M1$ shell model operator

$$\mathcal{M}(M1) = g(J_{\pi} - J_{\nu}). \tag{41}$$

This is also expressed in terms of ms RPA phonons and IBM bosons. Thus, one may use states having the IBM structure to compute the $M1$ transitions amplitudes. Figure 9 shows the results for the ratios

$$\begin{aligned} R_1(M1) &= \frac{B(M1, 1^+_{\rm ms} \to 2^+_2)}{B(M1; 1^+_{\rm ms} \to 0^+_1)}, \\ R_2(M1) &= \frac{B(M1, 2^+_{\rm ms} \to 2^+_1)}{B(M1; 1^+_{\rm ms} \to 0^+_1)}, \\ R_3(M1) &= \frac{B(M1, 2^+_{\rm ms} \to 2^+_1)}{B(M1; 1^+_{\rm ms} \to 2^+_2)}. \end{aligned} \tag{42}$$

A good agreement between theory and experiments is obtained for the ratio $R_1(M1)$. On the other hand, theory and experiments diverge in the estimates of $R_2(M1)$ and, especially, of $R_3(M1)$. This divergence originates from the strong discrepancy between computed and

measured strengths of the $2^+_{ms} \to 2^+_1$ $M1$ transition. As shown in figure 9, the behavior of the theoretical $B(M1; 2^+_{ms} \to 2^+_1)$ versus the mass number is just opposite to what is indicated by experiments, suggesting that the description of the one-phonon ms 2^+_{ms} is to be improved. The whole procedure should be reexamined in order to check if important ingredients are missing in the mapping process or to find the way of incorporating anharmonic features in the ms states.

5. Low-lying negative parity dipole excitations

It is a well-known fact that almost the total $E1$ strength is concentrated into the GDR lying at high energy, above $1\hbar\omega$. Relatively strong $E1$ transitions were nonetheless observed near the particle threshold in spherical nuclei and attributed to the so-called $E1$ pygmy dipole resonance (PDR) [128–136]. These excitations are properly described within approaches which go beyond the harmonic approximation. In fact, they were investigated within relativistic extensions of the RPA [30, 31] as well as within the QPM [137, 138].

At even lower energy, strong $E1$ transitions were detected in nuclear resonance fluorescence (NRF) experiments on spherical even–even nuclei near shell closures. The strength of these transitions is $\sim 10^{-3}$ W.u., orders of magnitude larger than the strengths normally measured in this energy region, which range from 10^{-5} to 10^{-6} W.u.. For a review and references, see [2, 3].

These low-lying 1^- states do not originate from the ph excitations building up the GDR. The experimental analysis [2, 139–147] has established that they have a more complex structure.

They are mainly characterized by the two-phonon component $|(2^+_1 \otimes 3^-_1)_{1^-}\rangle$ arising from the coupling between the collective quadrupole $|2^+_1\rangle$ and octupole $|3^-_1\rangle$ modes. In fact, in all cases, the excitation energies of these 1^- states roughly equal the sum of the energies of the two mentioned modes. Moreover, the $1^- \to 0^+_1$ $E1$ strengths reach their maximum values in nuclei with a closed proton or neutron shell and drop off sharply when moving away from shell closure. The reverse trend is observed for the $1^- \to 2^+_1$ $E1$ transitions, whose strengths are the lowest in magic nuclei and increase in going away from closed shells.

The quadrupole–octupole two-phonon structure qualifies these 1^- states as isoscalar. On the other hand, the $E1$ operator has an isovector character. This intriguing circumstance allows precious information to be drawn on the $\pi - \nu$ structure of these composite 1^- states from the analysis of the isovector $E1$ transitions.

Among the properties of the strong $E1$ transitions between low-lying states, the following one deserves special attention. The plot of the $|\langle 0^+_1 \| \mathcal{M}(E1) \| 1^-_1 \rangle|$ amplitudes versus the neutron number N presents a minimum at $N = 78$ or $N = 86$ in each chain of the Nd, Sm and Ba isotopes [148–150], consistently with a prediction made in RPA-based calculations [151]. All these isotopes have four valence neutron particles or holes. On the other hand, no minimum was observed in Xe isotopes [152] with four valence neutron holes. Thus, if existing, the minimum in these latter isotopes should occur at a larger number of neutron holes.

According to a very schematic IBM analysis [153–155], such a behavior results from a mutual cancellation of proton and neutron contributions to the $0^+_1 \to 1^-_1$ $E1$ transition. The phenomenological IBM approach, however, was not able to determine the position of the neutron minimum.

Microscopic investigations are therefore necessary in order to establish if and where the minimum occurs and to determine its position. These studies must be reliable. Thus, they have to reproduce the experimental data. More specifically:

(i) the calculation should yield a ratio $B(E1; 1_1^- \to 0_1^+)/B(E1; 3_1^- \to 2_1^+) \approx 1$, at least in the vicinity of magic nuclei;
(ii) in going away from shell closures, the computed $B(E1; 1_1^- \to 2_1^+)$ strength should increase, while the $B(E1; 0_1^+ \to 1_1^-)$ should reach a minimum at some value of the neutron number N when moving off the semimagic nuclei;
(iii) the $E1$ transition from the octupole 3^- to the mixed-symmetry $2^+_{\rm ms}$ states should be much stronger than the corresponding transition to the symmetric 2_1^+, namely $B(E1; 3_1^- \to 2^+_{\rm ms}) \gg B(E1; 3_1^- \to 2_1^+)$ and
(iv) the $E1$ strength should increase with quadrupole and octupole deformation, namely $B(E1; 0_1^+ \to 1_1^-) \propto \langle\beta_2^2\rangle\langle\beta_3^2\rangle$.

The behavior of $|\langle 0_1^+ \|\mathcal{M}\| 1_1^-\rangle|$ versus the neutron number was studied within the fermionic Q-phonon scheme [155, 156], which came out to be an efficient tool for the analysis of the low-lying collective states of both positive and negative parities and, in particular, of the 1^- states.

5.1. Q-phonon description of low-lying 1^- states in spherical nuclei

The Q-phonon scheme, aside from yielding simple and physically transparent relations between transition amplitudes, can be applied to nuclei far away from the region of validity of the harmonic approximation.

In order to keep memory of the microscopic structure, we adopt the fermionic Q-phonon scheme. This is analogous to the corresponding bosonic approach adopted within the IBM, discussed in section 3. The Q operators, however, have a fermionic structure.

The states of spin λ and parity π have the following expression:

$$|\lambda^\pi \mu\rangle = \mathcal{N}_\lambda \hat{Q}_{\lambda\mu}|0_1^+\rangle, \tag{43}$$

where the multipole operator is expressed in the fermionic form

$$\hat{Q}_{\lambda\mu} = \sum_{jj'mm'} \langle jm|r^\lambda Y_{\lambda\mu}|j'm'\rangle a^+_{jm} a_{j'm'} \tag{44}$$

and the normalization constant is given by

$$\mathcal{N}_\lambda = \frac{\sqrt{2\lambda+1}}{|\langle 0_1^+ \|Q_\lambda\|\lambda^\pi\rangle|}. \tag{45}$$

We consider the quadrupole and octupole states

$$|2_1^+, \mu\rangle = \mathcal{N}_2 \hat{Q}_{2\mu}|0_1^+\rangle, \qquad |3_1^-, \mu\rangle = \mathcal{N}_3 \hat{Q}_{3\mu}|0_1^+\rangle, \tag{46}$$

respectively. According to RPA calculations [34], such a simple phonon structure is well suited to describe the lowest excited 2_1^+ and 3_1^- states. These are also shown to collect most of the $E2$ and $E3$ strengths from the ground state.

The analysis of the experimental data suggests that the 1_1^- state should be composed of quadrupole and octupole collective operators, Q_2 and Q_3, so that

$$|1_1^-, M\rangle = \mathcal{N}_{1_1^-}(\hat{Q}_2 \times \hat{Q}_3)_{1M}|0_1^+\rangle. \tag{47}$$

The normalization factor is given approximately by $\mathcal{N}_{1_1^-} \approx \mathcal{N}_{2_1^+}\mathcal{N}_{3_1^-}$, if we neglect contributions from mixing terms whose contribution resulted to be less than 1% [157].

The $|1_1^-, M\rangle$ states (47) can be written in terms of the RPA collective phonons and the dominant two-quasiparticle components of the non-collective RPA solutions. The resulting formula shows that the $|1_1^-, M\rangle$ has a dominant two-phonon component built of one quadrupole and one octupole collective RPA phonons, a three-phonon component composed of two

collective quadrupole phonons coupled to one collective octupole RPA phonon and two-quasiparticle 1^- components. Given its complex structure, such a state should be compared with calculations which extend RPA so as to include anharmonic effects.

As we approach a deformed region, the 1^- levels split into a $K = 0$ and $K = 1$ band heads. In order to describe these two branches, we need to admix the $|1_1^-, M\rangle$ given by (47) with the Q-phonon component $[(Q_2 \times Q_2)_4 \times Q_3]_{1M}|0_1^+\rangle$. This mixing is large in deformed nuclei, about 70% for one component and 30% for the other. It is much smaller near spherical regions. In transitional nuclei with soft γ-modes, also the Q-phonon state $[(Q_2 \times Q_2)_2 \times Q_3]_{1M}|0_1^+\rangle$ becomes important.

The simple structure of the states allows relations to be derived between transition amplitudes which are valid also outside of the analytically solvable harmonic vibrator and rotor limits. Using, indeed, the model states just constructed, it is possible to compute the transition amplitude

$$\langle 1_1^-, M|\mathcal{M}_{1M}(E1)|0_1^+\rangle = \mathcal{N}_{1_1^-}\langle 0|(Q_2 \times Q_3)_{1M}\mathcal{M}_{1M}(E1)|0_1^+\rangle. \tag{48}$$

By making use of the Wigner–Eckart theorem, we obtain after some Racah algebra

$$\langle 1_1^-\|\mathcal{M}(E1)\|0_1^+\rangle = \langle 3_1^-\|\mathcal{M}(E1)\|2_1^+\rangle, \tag{49}$$

which yields

$$B(E1; 1_1^- \to 0_1^+)/B(E1; 3_1^- \to 2_1^+) = \tfrac{7}{3}. \tag{50}$$

This ratio coincides with that obtained in the harmonic limit, although no harmonic assumption was made here. The value obtained is only qualitatively consistent with the experimental one, of the order 1–2. This discrepancy suggests the presence of some admixtures in the $|1_1^-\rangle$, $|2_1^+\rangle$ and $|3_1^-\rangle$ states not taken into account in the Q-phonon scheme. It must be also mentioned that, at least in one experiment [158], a very small $B(E1; 3_1^- \to 2_1^+)$ was obtained yielding a ratio much larger than 7/3.

By analogous algebraic manipulations we obtain

$$\frac{\langle 1_1^-\|\mathcal{M}(E1)\|2_1^+\rangle}{\langle 1_1^-\|\mathcal{M}(E1)\|0_1^+\rangle} = \sqrt{\frac{5}{3}}\frac{\langle 1_1^-\|Q_2\|1_1^-\rangle}{\langle 0_1^+\|Q_2\|2_1^+\rangle}. \tag{51}$$

Since the quadrupole moment of the 1_1^- state can be expressed approximately in terms of the quadrupole moments of the 2_1^+ and 3_1^- states, we obtain

$$\frac{\langle 1_1^-\|\mathcal{M}(E1)\|2_1^+\rangle}{\langle 1_1^-\|\mathcal{M}(E1)\|0_1^+\rangle} \approx \frac{1}{\sqrt{35}\langle 0_1^+\|Q_2\|2_1^+\rangle}[\langle 2_1^+\|Q_2\|2_1^+\rangle + \sqrt{6}\langle 3_1^-\|Q_2\|3_1^-\rangle]. \tag{52}$$

The above formula explains why the $1_1^- \to 2_1^+$ transition gets enhanced with respect to the $1_1^- \to 0_1^+$ transition as we move away from magic or semimagic nuclei. It is simply because the quadrupole moments of the first 2_1^+ and 3_1^- increase as we depart from shell closures.

The above ratio deviates from the Alaga rule indicating that other components, like $(|4_1^+\rangle \otimes |3_1^-\rangle)_1$, enter the composite $|1_1^-\rangle$ state.

5.2. IBM analysis

An immediate insight into the underlying physics can be gained from an analysis based on the IBM [153, 154]. It is more convenient to evaluate the matrix element $\langle 3_1^-\|\mathcal{M}(E1)\|2_1^+\rangle$. This automatically yields the $\langle 1_1^-\|\mathcal{M}(E1)\|0_1^+\rangle$ amplitude, in virtue of equality (49).

As pointed out already, the IBM $|2_1^+\rangle$ and $|3_1^-\rangle$ states are $\pi - \nu$ symmetric and, therefore, have maximum F-spin ($F = F_{\max}$). The dipole transition operator $\mathcal{M}(E1)$ is mainly an F-spin vector. If it is assumed to be exactly an F-spin vector, we obtain

$$\langle 3_1^-\|\mathcal{M}(E1)\|2_1^+\rangle \sim (N_\pi - N_\nu). \tag{53}$$

According to this formula, only protons will contribute in a nucleus with a closed neutron shell. As valence neutron pairs are added, neutrons also contribute and tend to counteract the protons. A minimum value at $N_\pi = N_\nu$ is reached eventually.

For the transition from the symmetric 3_1^- to the mixed-symmetry $2_{\rm ms}^+$ state with $F = F_{\rm max} - 1$, an IBM calculation [154] yields

$$\langle 3_1^- \| \mathcal{M}(E1) \| 2_{\rm ms}^+ \rangle \sim \sqrt{\frac{N_\pi N_\nu}{(2N_\pi + 2N_\nu - 1)(N_\pi + N_\nu)}}. \tag{54}$$

Clearly, no cancellation between proton and neutron contributions occurs, suggesting a possible reason why the $\langle 3_1^- \| \mathcal{M}(E1) \| 2_{\rm ms}^+ \rangle$ amplitudes are large.

This merely phenomenological analysis cannot determine the minimum value of neutron and proton pair numbers. In fact, the physical $E1$ transition operator is not a pure F-spin vector. Moreover, the IBM cannot account for possible changes in the microscopic structure of proton and neutron bosons from nucleus to nucleus.

A similar result is obtained in the Q-scheme, where the ms 2^+ state is given by

$$|2_{\rm ms}^+\rangle = \left(\frac{Q_2^\nu}{\langle 0_1^+ | (Q_2^\nu Q_2^\nu)_0 | 0_1^+ \rangle^{1/2}} - \frac{Q_2^\pi}{\langle 0_1^+ | (Q_2^\pi Q_2^\pi)_0 | 0_1^+ \rangle^{1/2}} \right) |0\rangle. \tag{55}$$

Since the proton and neutron components have the same sign, the action of the F-spin vector $E1$ operator is constructive. It is, instead, destructive when acting on the symmetric $|2_1^+\rangle$. Indeed, using expression (55) for $|2_{\rm ms}^+\rangle$ in (54), after commuting the $E1$ operator with the quadrupole ones, we obtain the inequality

$$|\langle 3_1^- \| \mathcal{M}(E1) \| 2_{\rm ms}^+ \rangle| \gg |\langle 3_1^- \| \mathcal{M}(E1) \| 2_1^+ \rangle|. \tag{56}$$

In virtue of (49), we also have

$$|\langle (3_1^- \otimes 2_{\rm ms}^+)_1 \| \mathcal{M}(E1) \| 0_1^+ \rangle| \gg |\langle (3_1^- \otimes 2_1^+)_1 \| \mathcal{M}(E1) \| 0_1^+ \rangle|. \tag{57}$$

The last inequality seems to be non-consistent with the analytical result obtained in [153] within the sdf IBM2. In this latter approach, the $E1$ operator contains a two-body piece with proton and neutron components of the same sign. Our shell-model-based $E1$ operator is basically isovector so that the isoscalar contribution comes only from the small component proportional to $(N - Z)/A$, necessary to subtract the spurious contribution due to the center of mass motion.

5.3. Effect of the RPA ground-state correlations

The dipole transition amplitude $\langle 1_1^- \| \mathcal{M}(E1) \| 0_1^+ \rangle$ may be be evaluated using expressions (43) and (47) for the state vectors $|2_1^+\rangle$, $|3_1^-\rangle$ and $|1_1^-\rangle$

$$|2_1^+, \mu\rangle = \tilde{\mathcal{N}}_{2_1^+} \hat{Q}_{2\mu} |0_1^+\rangle_{\rm RPA}, \tag{58}$$

$$|3_1^-, \mu\rangle = \tilde{\mathcal{N}}_{3_1^-} \hat{Q}_{3\mu} |0_1^+\rangle_{\rm RPA}, \tag{59}$$

$$|1_1^-, M\rangle = \tilde{\mathcal{N}}_{1_1^-} (\hat{Q}_2 \times \hat{Q}_3)_{1M} |0_1^+\rangle_{\rm RPA}, \tag{60}$$

where now $|0_1^+\rangle_{\rm RPA}$ is a RPA-correlated ground state. The use of such a state is legitimate since the derivation of the ratios (50) and (52) relies only on the Q-phonon form of the state vectors, independent of the actual structure of the 0_1^+ state.

We assume that the ground state contains only those correlations which are produced by the quadrupole–quadrupole and octupole–octupole interactions. The quadrupole and octupole interaction strength constants are fixed so as to reproduce the experimental values of

$B(E2; 0_1^+ \to 2_1^+)$ and $B(E3; 0_1^+ \to 3_1^-)$, respectively. The ground-state correlations induced by the dipole–dipole interaction are not included. Thus, in calculating the $E1$ transition strength, we must introduce the core polarization factor χ which comes from the coupling of the low-lying excitations with the GDR [1]. RPA-like calculations of the E1 transitions were performed in [151, 159–161].

When the RPA-correlated ground state is included in (58) and (59), the $|2_1^+\rangle$ and $|3_1^-\rangle$ states assume the microscopic structure

$$|2_1^+, \mu\rangle = \tilde{\mathcal{N}}_{2_1^+}\left(b_{2\mu}^+ - \frac{2\sqrt{21}}{P(2)}\sum_{ss'} W_{ss'}(3)\left[\left(\alpha_s^+ \times \alpha_{s'}^+\right)_1 \times b_3^+\right]_{2\mu}\right)|0\rangle, \tag{61}$$

$$|3_1^-, \mu\rangle = \tilde{\mathcal{N}}_{3_1^-}\left(b_{3\mu}^+ + \frac{2\sqrt{15}}{P(3)}\sum_{ss'} W_{ss'}(2)\left[\left(\alpha_s^+ \times \alpha_{s'}^+\right)_1 \times b_2^+\right]_{3\mu}\right)|0\rangle, \tag{62}$$

where ($F_\lambda = i^\lambda r^\lambda Y_\lambda$)

$$W_{ss'}(3) = \sum_t \langle t\|F_2\|s\rangle(-1)^{j_t+j_{s'}}(u_t u_s - v_t v_s)\begin{Bmatrix} 3 & 2 & 1 \\ j_s & j_{s'} & j_t \end{Bmatrix}\varphi_{ts'}^{(3)},$$

$$W_{ss'}(2) = \sum_t \langle t\|F_3\|s\rangle(-1)^{j_t+j_{s'}}(u_t u_s - v_t v_s)\begin{Bmatrix} 2 & 3 & 1 \\ j_s & j_{s'} & j_t \end{Bmatrix}\varphi_{ts'}^{(2)},$$

$$P(\lambda) = \sum_{ss'}\langle s\|F_\lambda\|s'\rangle(u_s v_{s'} + u_{s'} v_s)\left(\psi_{ss'}^{(\lambda)} + \varphi_{ss'}^{(\lambda)}\right).$$

The operators $b_{2\mu}^\dagger$ and $b_{3\mu}^\dagger$ create the most collective quadrupole and octupole RPA phonons defined by the amplitudes $\psi_{ss'}^{(\lambda)}$ and $\varphi_{ss'}^{(\lambda)}$ corresponding to the first roots of the RPA secular equation; $\alpha_s^\dagger$ are the quasiparticle creation operators determined by the coefficients u and v of the Bogoliubov transformation.

Given the absence of dipole–dipole correlations in the ground state, no 1^- phonon appears. It follows that the 1_1^- state has a composite structure whose components are $(b_2^+ \times b_3^+)_1|0\rangle$ and $\sum_{ss'} W_{ss'}(\lambda)(\alpha_s^+\alpha_{s'}^+)_1|0\rangle$ (with $\lambda = 2, 3$). The bosonic component is by far the dominant one. Its contribution to the norm is close to 100%.

The 1^- two-quasiparticle components are needed in order to have a complete basis. They are coupled to the RPA phonons by the quasiparticle–phonon coupling term of the QPM Hamiltonian [34, 151, 157, 159–161]. As we shall see, they give a sizable contribution even if their weight is small (∼1%). There are also other components in the 2_1^+, 3_1^- and 1_1^- states. They are, however, small and of no relevance to the $E1$ transitions [159]. These are given by

$$\langle 1_1^-\|\mathcal{M}(E1)\|0_1^+\rangle = e_{\text{eff}}\sqrt{\frac{4\pi}{3}}\left[\left(1 + \frac{N-Z}{A}\right)B_\pi - \left(1 - \frac{N-Z}{A}\right)B_\nu\right], \tag{63}$$

where the effective charge $e_{\text{eff}} = \frac{e}{2}(1+\chi)$ accounts for polarization effects incorporated in χ [1], and B_π and B_ν are microscopic quantities which incorporate the contribution coming from the quadrupole–octupole phonons and the phonon–quasiparticle interference terms present in the 2^+ and 3^+ states (61) and (62). Their involved formulas can be found in [155]. Apparently, the transition amplitude depends on the balance between these proton and neutron quantities B_π and B_ν.

The trend of the $0^+ \to 1^-$ $E1$ transition amplitudes with the mass number is illustrated in the plots of figures 10 and 11 for several chains of isotopes. One may note that the measured amplitudes are either close or just above the theoretical quantities when computed

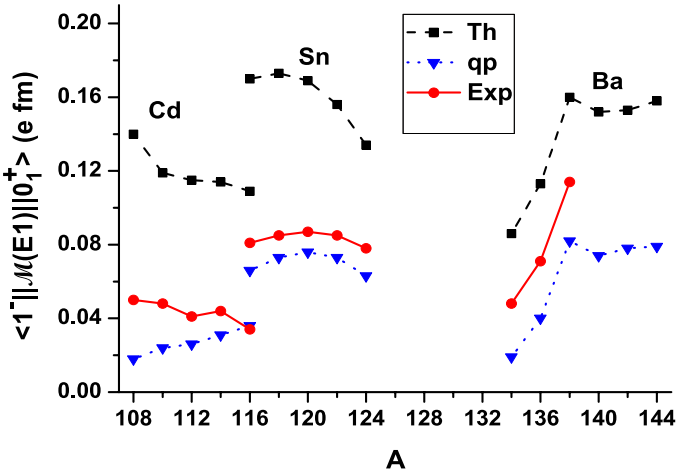

Figure 10. Theoretical (dashed line) versus experimental (solid line) E1 $0_1^+ \rightarrow 1_1^-$ absolute reduced amplitudes in Cd, Sn and Ba (from [155]). The dot line gives the contribution obtained once the two-quasiparticle admixtures are eliminated.

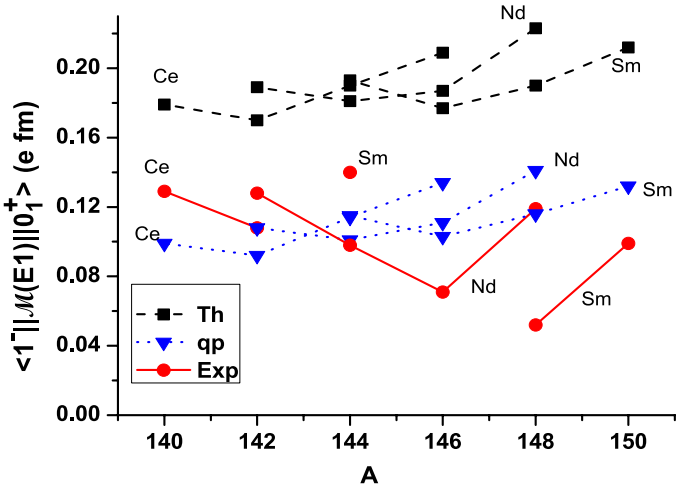

Figure 11. The same as in figure 10, but for Ce, Nd and Sm isotopes (from [155]).

without the two-quasiparticle admixture to the collective quadrupole–octupole two-phonon component.

The two-quasiparticle components, though accounting for less than 1%, considerably enhance the transition amplitudes with respect to the measuring quantities. This result suggests that their contribution is overestimated. How to obtain a quenching is not straightforward given their small weight in the total wavefunction.

We may conclude by saying that the two-phonon component $(|2_1^+\rangle \otimes |3_1^-\rangle)_{1^-}$, which gives the main contribution to the norm of the $|1_1^-\rangle$ state, determines the excitation energy and the $E2$ and $E3$ decay properties of the $|1_1^-\rangle$ state. It is, nonetheless, necessary to include the contribution induced by the dipole two-quasiparticle components, although quenched with

Table 7. Proton (B_π) and neutron (B_ν) contributions to $\langle 1_1^- \| \mathcal{M}(E1) \| 0_1^+ \rangle$ (63) in Nd isotopes.

Nucleus	B_π (in fm)	B_ν (in fm)
$^{142}Nd_{82}$	0.78	0.17
$^{144}Nd_{84}$	0.80	0.21
$^{146}Nd_{86}$	0.87	0.26
$^{148}Nd_{88}$	1.05	0.32

respect to the present estimate, in order to obtain a satisfactory description of the electric dipole transition $0_1^+ \rightarrow 1_1^-$.

In both cases, the calculation reproduces the observed trend of the $E1$ transition amplitudes with the mass number. ^{146}Nd and ^{148}Sm represent a notable exception. These nuclei have a deep minimum when the number of valence neutrons $N_\nu = 4$, a fact already pointed out in the introduction. The calculation yields a shallow minimum for $N_\nu = 2$ instead.

In the case of the Nd and Sm isotopes, the A-dependence of $|\langle 0_1^+ \| \mathcal{M} \| 1_1^- \rangle|$ obtained in the microscopic calculations deviates from the one predicted by the IBM. As already pointed out, the IBM-reduced $E1$ transition amplitudes decrease, for a given number of valence proton pairs, as we add neutron pairs starting from the neutron closed shell. In the microscopic case, the same amplitudes increase with the neutron number starting from $N_\nu = 2$. In the microscopic scheme, the contribution to the $E1$ transition coming from protons changes even if their number is kept constant. In fact, the ground-state correlations change as the number of valence neutrons increases. This fact is illustrated in table 7, where the proton contribution B_π grows at the same rate of B^ν.

It is useful to relate the electric dipole two-quasiparticle component entering the 1_1^- state to the p-boson introduced within the IBM [162] to construct α-cluster dipole states. If disentangled from the other pieces of the 1_1^- state, this two-quasiparticle component can be normalized to one and then used to calculate the $E1$-reduced amplitude obtaining values of the order 0.6–0.7 e · fm. For comparison, we obtain approximately 6 e · fm for a pure α-cluster state and 1.7 e · fm for a 1p1h $(1h_{11/2}\ 1g_{9/2}^{-1})_{1^-}$ proton state. These numbers indicate that the correspondence of the two-quasiparticle admixtures in the microscopic 1_1^- state with the IBM p-boson is rather loose.

In conclusion, in order to account for the enhanced $E1$ transitions, it is necessary to go beyond the harmonic approximation. This necessity emerges clearly from the following example. In RPA only boson-allowed transitions are promoted. In this approximation, in fact, the one-body fermion operators contain only the $\alpha_s^\dagger \alpha_t^\dagger$ and $\alpha_s \alpha_t$ terms which change the number of quasiparticles by two units.

Thus, RPA cannot describe the $E1$ $3_1^- \rightarrow 2_1^+$ transition promoted by the boson-forbidden $\alpha_s^\dagger \alpha_t$ pieces. These terms should be included in the quadrupole and octupole operators Q_2, Q_3, thereby leading to the appearance of anharmonic terms in the Hamiltonian which contains quadrupole–quadrupole and octupole–octupole interactions. The inclusion of the terms in $\alpha_s^\dagger \alpha_t$ is necessary in order to preserve the commutation relations between Q_2, Q_3 and $\mathcal{M}(E1)$.

5.4. Neutron number dependence of the E1 transition amplitude

The approach outlined above may be adopted to study the trend of $B(E1; 0_1^+ \rightarrow 1_1^-)$ versus the number of neutrons. Dealing mainly with spherical nuclei, it is appropriate to describe the ground-state correlations in RPA.

Xe isotopes are a good test ground for analyzing the validity and the effect of this approximation. Heavier Xe isotopes are spherical. The treatment of their ground state in RPA

is therefore justified. For the study of the lightest transitional ^{124,126}Xe, it may be useful to be guided by the analogy between IBM and RPA.

In IBM, the lighter Xe isotopes belong to the O(6) dynamical symmetry limit. Thus, their ground state may be written as

$$|0_1^+\rangle = \sqrt{1 - c_1^2 - c_2^2 - \cdots}\frac{1}{\sqrt{N!}}(s^+)^N|0\rangle + c_1\frac{1}{\sqrt{2}}(d^+d^+)_0\frac{1}{\sqrt{(N-2)!}}(s^+)^{N-2}|0\rangle + c_2(d^+d^+d^+d^+)_0\frac{1}{\sqrt{(N-4)!}}(s^+)^{N-4}|0\rangle + \cdots, \quad (64)$$

where $|0\rangle$ is the boson vacuum and N is the maximum number of bosons.

In RPA, one may consider the following form:

$$|0_1^+\rangle = \sqrt{1 - c_1^2 - c_2^2 - \cdots}|0\rangle + c_1\tfrac{1}{\sqrt{2}}(A_2^+A_2^+)_0|0\rangle + c_2(A_2^+A_2^+A_2^+A_2^+)_0|0\rangle + \cdots, \quad (65)$$

where $|0\rangle$ is the quasiparticle vacuum and A_2^+ is the operator creating a collective superposition of two-quasiparticle states coupled to the angular momentum $L = 2$.

Thus, RPA and IBM ground states exhibit a similar structure if the bilinear fermion operator A_2^+ is put in correspondence with the d^+s boson operator.

They differ, of course, in the values of the coefficient c_i. In RPA, the main component of the ground-state wavefunction is the first term of (65) proportional to the quasiparticle vacuum. In the IBM, instead, the second term in (64) is in general dominant. This quantitative difference establishes the limit of validity of the use of a RPA-correlated ground state

In fact, using a consistent-Q IBM Hamiltonian, we found that RPA is adequate to describe the heavy $^{128-136}$Xe isotopes. It underestimates, instead, the ground-state correlations of the lighter ^{124,126}Xe. The state of these isotopes is better described as a combination of two lowest 0^+ RPA states. A visible effect of this mixture is the splitting of the $E1$ strength in two 1^- peaks.

We can now face the calculation of the reduced $E1$ transition amplitudes using (63). These depend critically on the competition between the proton and neutron contributions. We therefore consider first the behavior of B_π and B_ν with the neutron number. As shown in figure 12, in Xe isotopes the proton contribution is by far dominant in correspondence of the neutron shell closure ($N = 82$). The neutron quantity B_ν raises rapidly with the number of neutron holes. Though at a slower rate, however, also the proton piece increases, even if the number of protons is kept constant. In fact, the ground state gets more and more correlated as the number of neutron holes increases.

As a result, the difference $(B_\pi - B_\nu)$ decreases with the neutron number and reaches a minimum value at A=128. As A decreases further, $(B_\pi - B_\nu)$ changes sign but its absolute value increases. Thus, $|\langle 1_1^-\|\mathcal{M}\|0_1^+\rangle|$ has a minimum at A=128. According to our calculations, this occurs when the number of the neutron holes is equal to 8 (see figure 13).

A similar behavior is obtained in Nd and Sm isotopes. In these isotopes, the minimum occurs when the number of the valence neutrons or neutron holes is equal to 4.

The picture changes in the chain of $^{116-124}$Sn and $^{108-116}$Cd isotopes. In $^{116-124}$Sn, as shown in figure 12, B_π is almost vanishing throughout the whole chain and B_ν is large but varies slowly without following a monotonic behavior. Apparently, the shell closure inhibits the protons. These remain basically inert and affect the valence neutrons very little.

The same quantities B_π and B_ν undergo large variations with A in $^{108-116}$Cd, as shown in figure 12. Their trend, however, is similar. Both quantities have a minimum in correspondence of the neutron number $N = 60$ and, then, increase with A. The net result is that B_π and B_ν do

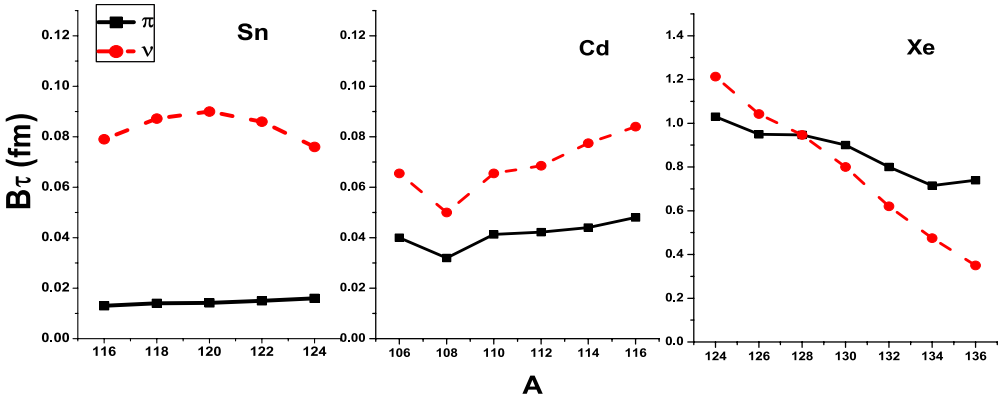

Figure 12. Proton (B_π) and neutron (B_ν) contributions to the $E1$ transition amplitudes in Sn, Cd and Xe isotopes (Reproduced with kind permission of Springer Science+Business Media from Jolos R V, Shirikova N Yu and Voronov V V 2006 On neutron number dependence of $B(E1;\ 0_1^+ \rightarrow 1_1^-)$ reduced transition probability *Eur. Phys. J.* A **29** 147).

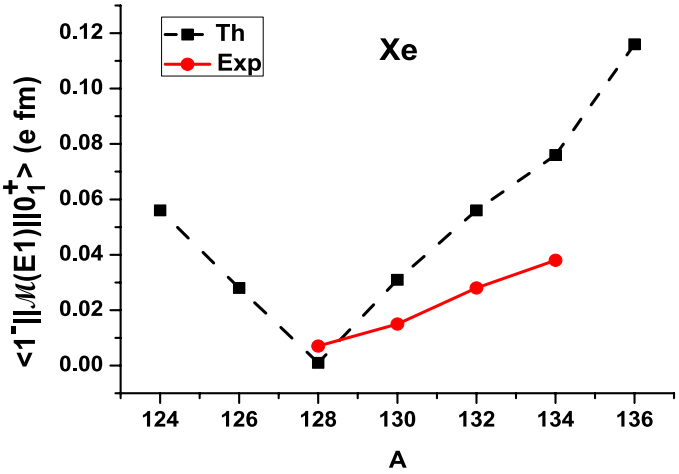

Figure 13. Experimental versus calculated electric dipole transition amplitudes in Xe isotopes (Reproduced with kind permission of Springer Science+Business Media from Jolos R V, Shirikova N Yu and Voronov V V 2006 On neutron number dependence of $B(E1;\ 0_1^+ \rightarrow 1_1^-)$ reduced transition probability *Eur. Phys. J.* A **29** 147).

not cross, since the neutron contribution remains larger for all isotopes. In these isotopes, the active proton holes are only two and, therefore, not effective enough in changing the collective behavior of the neutron-rich isotopes.

Going back to Xe isotopes, figure 13 shows that the $E1$-reduced amplitudes decrease in going from ^{136}Xe to ^{128}Xe, in agreement with the experiments [152]. The $E1$ amplitudes reach a minimum at $A = 128$ and, then, increase as the number of neutron holes increases.

The experimental situation for the isotopes with $A < 128$ is unclear. Strong dipole transitions were observed, but the parity was not determined. If they are assumed to be induced by low-energy octupole excitations [163], we deduce from the experimental reduced width $\Gamma_0^{\rm red}$ the amplitudes $|\langle 0_1^+ \| \mathcal{M} \| 1_1^- \rangle| = 0.051\mathrm{e}\cdot\mathrm{fm}$ for ^{124}Xe and $|\langle 0_1^+ \| \mathcal{M} \| 1_1^- \rangle| = 0.041\mathrm{e}\cdot\mathrm{fm}$ for ^{126}Xe. The first value is close to the calculated one; the second one is somewhat larger.

In the heavier Xe isotopes ($A > 128$), the calculation overestimates the $E1$ transition amplitudes, especially as we approach the magic neutron number $N = 82$ (figure 13). We may try to explain the results by observing that the strength of the $0_1^+ \to 1_1^-$ $E1$ transition is determined by the ground-state correlations. These are, in turn, determined by the collective properties of the octupole and quadrupole phonons. The collectivity of these phonons increases in Xe isotopes with an increasing number of neutron holes and, therefore, enhances both proton and neutron contributions. As we approach the shell closure, instead, the neutron correlations are not sufficiently accounted for by the nuclear forces we used. Thus, the neutron contribution B_ν is underestimated and the difference $(B_\pi - B_\nu)$ becomes too large.

In conclusion, by exploiting the Q-phonon scheme, it is possible to derive simple relations between different reduced matrix elements which qualitatively explain the trend and properties of the $E1$ transitions.

By treating the ground-state correlations in the RPA approximation and using the Q-phonon form of the 1_1^- states, we could fairly well reproduce the observed trend of the $0_1^+ \to 1_1^-$ $E1$-reduced amplitudes versus the neutron number and relate such a behavior to a competing contribution of protons versus neutrons.

Such a competition may yield a minimum which the calculation is able to determine. The occurrence of a minimum is not a general rule. It has been shown that this does not exist in chains of isotopes due to their specific shell structure.

It has been also shown that the two-quasiparticle components of the $|1_1^-\rangle$ state, though small, should be taken into account in order to achieve a fair agreement with the experimental data.

6. QPM in deformed nuclei

In deformed nuclei, the QPM states are characterized by the quantum number K^π. In general it is sufficient to include up to two phonons to study their spectroscopic properties. Thus, the generic intrinsic state has the structure

$$\Psi_{nK^\pi} = \sum_i C_i^{(n)} |i, K^\pi\rangle + \sum_{v_1 v_2} C_{v_1 v_2}^{(n)} |[v_1\, v_2]_{K^\pi}\rangle, \tag{66}$$

where $v_i = i\lambda_i\mu_i$, and λ and μ give the multipolarity and magnetic component of the phonon operators.

The QPM was adopted extensively to study the low-lying properties of deformed nuclei. It has provided a thorough description of the low-lying $M1$ excitations associated with the scissor mode [66, 67] (see [68–70] for an exhaustive review). Indeed, by accounting for the quenching and fragmentation induced by the PC, it was possible to reproduce with fair accuracy the fine structure as well as the magnitude of the $M1$ strength throughout the nuclei of the rare-earth region [164, 165].

The QPM gave a crucial contribution to the understanding of the low-energy enhanced $E1$ transitions [2] by correlating them to octupole vibrations [165]. A QPM review of $E1$ and $M1$ low-lying transitions can be found in [166, 167].

Here we concentrate our review on the QPM analysis of the 0^+ states, which attracted great attention in recent years.

6.1. 0^+ *states in deformed nuclei*

In the past, several experimental and theoretical studies have thoroughly examined the properties of the low-lying 0^+ excitations in order to verify if some of them exhibit the typical properties of a β vibrational mode [168]. The results were controversial and not conclusive.

Nonetheless, these studies lead to a discovery of great interest. A large number of low-lying excited 0^+ levels were observed in ^{158}Gd through a high resolution (p, t) experiment [39]. Such a large number was not peculiar of ^{158}Gd. Copious 0^+ levels were detected in actinide nuclei [40], in ^{168}Er [41] and in several other nuclei [42–44]. The number of 0^+ states detected in ^{168}Er is particularly large, the levels below 4 MeV amounting to about 30 [41].

The distribution pattern of the two-nucleon transfer transition strengths shows that one single 0^+ state is strongly populated in all nuclei, with the exception of ^{168}Er where the strength is fragmented into several small peaks.

The first theoretical investigation [169] was carried out within the IBM. Since standard IBM and other collective models could yield a very small number of 0^+ levels, it was necessary to use the extended (sdpf) IBM in order to account for a large fraction of the detected 0^+ states. The (sdpf) IBM analysis points out the importance of the octupole degrees of freedom. In fact, several 0^+ levels were associated with collective octupole two-boson IBM states.

The first microscopic analysis was performed in the framework of the projected shell model [170] adopting a restricted space spanned by two- and four-quasiparticle states. Including the latter states was crucial for covering the whole spectrum. The calculation reproduced all the energy levels well.

Exhaustive investigations of these states were carried out within the QPM through the calculation of energies, electromagnetic transition strengths and two-nucleon transfer spectroscopic factors [171–173]. The normalized monopole strength

$$\rho^2\big(E0; 0_n^+ \to 0_1^+\big) = \frac{1}{e^2R_0^4}\left|\langle 0_1^+|\sum_k e_{\rm eff}(k) r_k^2|0_n^+\rangle\right|^2 \tag{67}$$

was computed in addition to the quadrupole one $B(E2; 0_n^+ \to 0_0^+)$.

The most important information comes from the two-nucleon transfer spectroscopic factors

$$\mathcal{S}_n(p,t) = \left(\frac{\Gamma_n(p,t)}{\Gamma_0(p,t)}\right)^2, \tag{68}$$

where

$$\Gamma_n(p,t) = \langle 0_n^+, N-2|\sum_q^{(\tau=\nu)} a_q a_{\bar{q}}|0_1^+, N\rangle = \sum_i C_i^{(n)}\Gamma_i(p,t) \tag{69}$$

are the QPM (p, t) transfer amplitudes. The $\Gamma_i(p, t)$ amplitudes include the *allowed* transitions to the one-phonon components $|i, K^\pi = 0^+\rangle$ of the QPM state (66) as well as the *forbidden* transitions from the ground to the two-phonon components $|[\nu_1\,\nu_2]_{0^+}\rangle$. The two-phonon contribution, however, came out to be negligible, so that the full strength is carried by the one-phonon allowed transitions. Thus, the amplitudes are basically given by

$$\Gamma_i(p,t) \simeq -2\sum_{qq'}^{\tau=\nu}\left[\psi^i_{qq'}v_q v_{q'} - \phi^i_{qq'}u_q u_{q'}\right], \tag{70}$$

where u_q and v_q are the occupation number coefficients of the Bogoliubov transformation.

The two-nucleon spectroscopic factors are directly extracted from the experiments and represent a unique probe for pairing correlations. The effect of pairing, indeed, is to enhance the cross sections of the 0^+ two-nucleon reactions. Thus, the superfluid ground states of nuclei far from shell closure, in particular the well-deformed ones, are strongly populated in (p, t) and (t, p) reactions, due to the large overlap of the wavefunctions between N and $N \pm 2$ nuclei. The same reactions may also appreciably populate excited 0^+ states. These, being induced by the fluctuations of the pairing field in the ground state, describe pairing vibrational modes [174, 175].

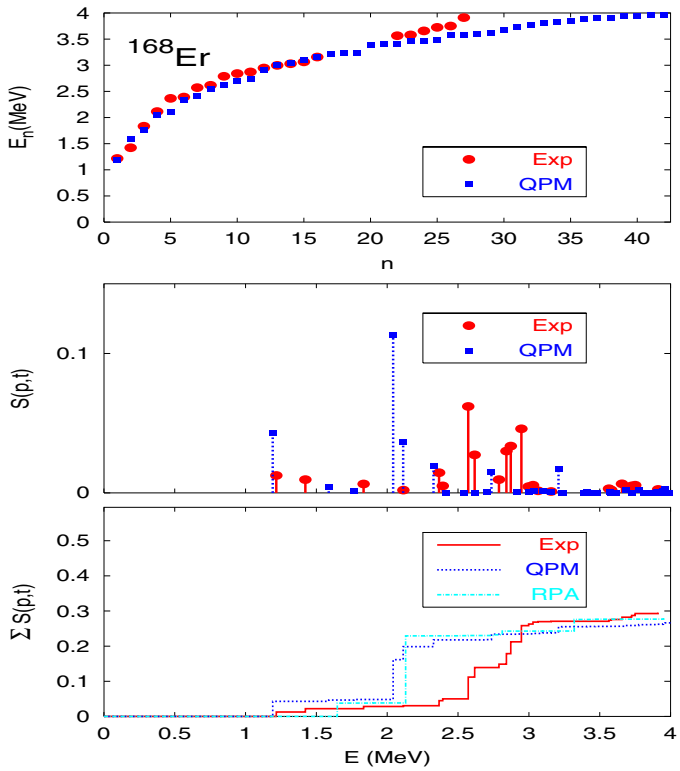

Figure 14. QPM versus experimental data in ^{168}Er (from [172]). These include the energies of the 0^+ states (top panel), the energy distribution of the (p, t) spectroscopic factors (middle) and their running sum (bottom). The experimental data are taken from [41].

The QPM calculation yields, in general, more 0^+ states than the ones observed. In ^{168}Er, for instance, the QPM levels are ∼40 below 4 MeV, to be compared with the ∼30 levels detected experimentally (see top panel of figure 14). On the other hand, all the 0^+ states in excess carry a negligible (p, t) strength (second panel) and, therefore, cannot be observed. The calculation reproduces the experimental energies fairly well, with the exception of few levels in the high-energy sector which are underestimated.

Almost all the 0^+ excitations below 3 MeV in ^{168}Er are described by one-phonon states which, in some cases, are rather fragmented. Only one, in this energy range, is a two-phonon state built of a phonon with high multipolarity. The weight of the two-phonon components becomes appreciable just above 3 MeV and increases more and more with the energy. The octupole phonons do not play any special role, except for a few states above 3 MeV, where they are dominant.

The computed strength of the $E2$ decay transition from the 0^+_2 bandhead to the 2^+ of the ground band is small. One obtains, in fact, $B_{\rm QPM}(E2; 0^+_2 1 \to 2^+_1) = 0.11$ W.u., in agreement with the experimental value $B_{\rm exp}(E2; 0^+_2 \to 2^+_1) = 0.08(1)$ W.u. [176]. The $E2$ decay strengths of the other 0^+ states are even smaller. Also the normalized monopole transitions are generally weak. The strength collected by the bandhead 0^+_2 is $\rho^2_{\rm QPM}(E0; 0^+_2 \to 0^+_1) = 1.48 \times 10^{-3}$ close to the experimental value $\rho^2_{\rm exp}(E0; 0^+_2 \to 0^+_1) = 0.8(8) \times 10^{-3}$ [177–179]. We therefore find an almost complete lack of quadrupole collectivity in all 0^+ states of ^{168}Er.

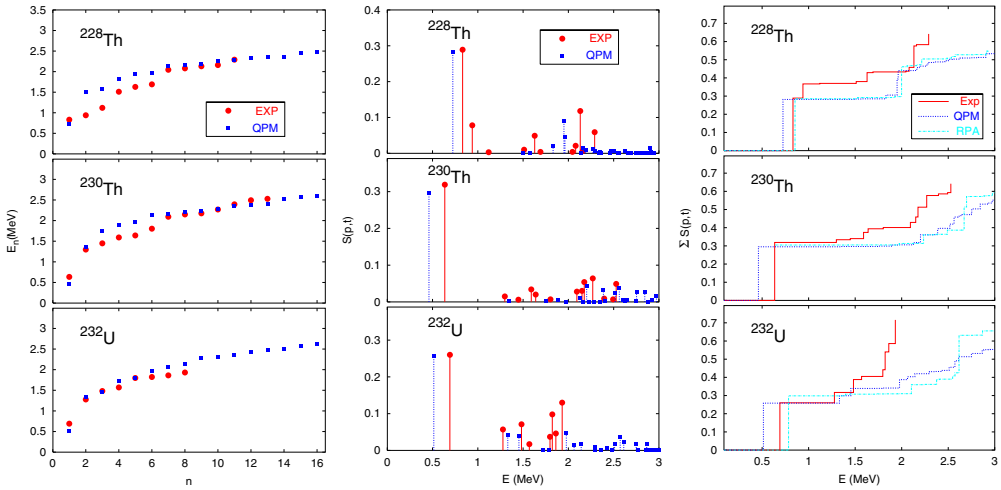

Figure 15. Energy levels (left), energy distribution (middle) and running sum (right) of (p, t) spectroscopic factors in the actinides (from [172]). The experimental data are taken from [40].

All these states, indeed, are composed almost solely of pairing correlated $q\bar{q}$ components. Pairing, however, acts coherently only into one RPA 0^+ state. This collects most of the two-nucleon transfer strength $\mathcal{S}(p, t)$. In the QPM, however, the coupling with the other phonons depletes the (p, t) strength of the collective RPA 0^+ state, yielding a fragmented spectrum reasonably close to the experimental data (middle panel of figure 14).

Important discrepancies still remain in the height of the main peak and in the strength distribution. The computed spectrum is shifted downward with respect to the experimental one. These discrepancies are manifested even more in the bottom panel of figure 14 showing that both the RPA and QPM strengths reach saturation too early with respect to experiments. The insufficient damping of the highest 0^+ RPA peak may be traced back to the truncation of the two-phonon space. Configurations which couple appreciably to the 0^+ RPA phonons might have been excluded. Nonetheless, the QPM strength sums up to a value ~ 0.25, which closely approaches the experimental integrated strength.

The calculation yields very little strength above 3 MeV, consistent with experiments. The levels above 3 MeV correspond predominantly to two-phonon excitations and are, therefore, poorly populated in transfer reactions.

Figure 15 (left panel) shows that the QPM calculation reproduces fairly well the experimental energy levels in ^{232}U, ^{230}Th and ^{228}Th.

The $E2$ and, especially, the $E0$ strengths in the actinides are generally larger than the corresponding quantities in ^{168}Er by at least one order of magnitude. In ^{230}Th, for instance, the computed $E2$ strength is $B^{(\mathrm{QPM})}(E2; 0_2^+ \to 2_1^+) = 1.71$ W.u., fairly close to the measured value $B^{(\mathrm{exp})}(E2; 0_2^+ \to 2_1^+) = 1.10$ W.u. [180]. The monopole transition strength collected by the first excited 0^+ is $\rho^2_{\mathrm{QPM}}(E0; 0_2^+ \to 0_1^+) = 8.2 \times 10^{-3}$, smaller than the value $\rho^2_{\mathrm{exp}}(E0; 0_2^+ \to 0_1^+) = 50(20) \times 10^{-3}$ extracted from experiments [179].

As shown in the middle panel of figure 15, the QPM normalized spectroscopic factors $\mathcal{S}(p, t)$ are in fair agreement with experiments. The calculation yields one strong peak close in magnitude to the corresponding experimental value, while other peaks are small consistently with experiments. These are typical features of a pairing vibrational mode.

Both RPA and QPM strengths reach saturation at higher energy with respect to experiments. This discrepancy may be related to a mismatch between the QPM and

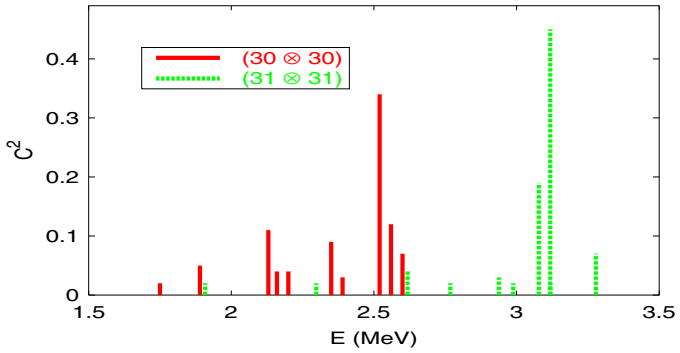

Figure 16. Strength distribution of the two lowest octupole two-phonon components among different QPM 0^+ states in ^{230}Th (from [172]).

experimental levels and may be cured by including hexadecapole and spin–quadrupole pieces in the ph two-body potential. The spin–quadrupole interaction, in particular, was shown to push an additional RPA 0^+ level below the pairing gap in the actinides [181].

The octupole phonons, though observed at low energies in the actinides, have a modest impact on the 0^+ states, at variance with the IBM prediction [40]. The theory yields, indeed, low-lying unperturbed octupole RPA two-phonons. On the other hand, the enforcement of the Pauli principle according to the prescription discussed in section 2 spoils the octupole coherence and yields a spreading of the octupole–octupole phonon components among several QPM 0^+ states. It follows that the strength of the two lowest octupole–octupole phonons gets redistributed among many closely packed QPM 0^+ states and pushed at higher energy. Such a mechanism is illustrated in figure 16 for ^{230}Th.

Transfer reaction experiments have populated in large abundance also states with $J^\pi = 2^+$ in ^{168}Er [41] and, more recently, states with $J^\pi = 2^+$ and higher spins in ^{230}Th [182]. Several of them belong to rotational bands based on 0^+ states. Others were interpreted as vibrational excitation modes. This assumption was supported by QPM calculations that strongly predict excited levels close to the observed ones. The QPM accounts for all states observed in ^{168}Er but underestimates the number of states in ^{230}Th. On the whole, it yields energies and (p, t) strengths in fair agreement with the data for both nuclei.

The QPM was applied to the $^{188-192}$Os isotopes in order to investigate the evolution of the properties of 0^+ states as one moves from well-deformed toward transitional nuclei [173]. A major finding was that the QPM 0^+ states are a mixture of several QRPA 0^+ phonons with a $\gamma\gamma$ two phonon component, in addition

$$|0^+\rangle \sim \sum_k c_k |0^+_k\rangle_{\mathrm{RPA}} + c_{22}|2^+_\gamma 2^+_\gamma\rangle. \tag{71}$$

This mixing increases in going from A=188 to the heavier isotopes and is to be contrasted with the purity of the 0^+ states in the well-deformed regions discussed previously ($|0^+\rangle_{\mathrm{QPM}} \sim |0^+_k\rangle_{\mathrm{RPA}}$). The increasing fragmentation with the mass number reflects the fact that we are approaching the γ-soft region. A consequence of this mixing is an overall quenching of the two-nucleon transfer spectroscopic factors. The computed summed strengths are $\sum_n S_n(p,t)_{\mathrm{QPM}} \sim 0.09 - 0.10$, comparable to the values $\sum_n S_n(p,t) \sim 0.12$–$0.15$ extracted from the experimental normalized cross sections [44]. Both values are considerably smaller than the integrated spectroscopic factors in well-deformed nuclei. For ^{158}Gd and ^{168}Er, in

fact, the QPM yielded $\sum_n S_n(p,t)_{\rm QPM} \sim 0.25$ in very good agreement with the measured values.

7. Concluding remarks

The review has shown that low-lying spectroscopic properties in vibrational and well-deformed nuclei can be investigated thoroughly within the QPM. Like the IBM, the QPM satisfactorily describes the gross properties of the low-lying spectra which vary smoothly with the number of neutrons (protons) along a chain of isotopes (isotones) in the vicinity of proton (neutron) shell closures.

Moreover, it accounts for features which are manifestation of the specific shell structure of a given nucleus. An example of this kind was provided by the different origin of the fragmentation of the $M1$ response in nuclei above and below the neutron magic number $N = 82$, resulting from a subtle interplay between pairing and subshell closures in the $N = 80$ isotones and from a PC in the $N = 84$ isotones.

The close correspondence with the IBM has enabled us to embed, by a mapping procedure, the QPM and RPA states into the IBM formalism and, thereby, successfully perform microscopic studies of low-lying collective excitations in transitional regions, not directly accessible to the QPM.

An important example is provided by the behavior of the $E1$ $0^+_1 \rightarrow 1^-_1$ transition amplitudes versus the neutron number. Such a RPA-based scheme reproduces the observed trend with fair accuracy and shows that such a behavior results from a competition between proton and neutron contributions. In Xe isotopes, for instance, the $E1$ transition amplitude decreases with the number of neutron holes, in agreement with the experimental data [140], until it reaches a minimum and, then, increases again.

The model is also able to determine the position of such a minimum and predict a threshold in the number of protons for its occurrence. It has established, for instance, that no minimum exists in Sn and Cd isotopes due to insufficient number of valence protons.

On the other hand, the microscopically based IBM analysis fails to account for other properties. It yields, for instance, contradictory results on the $M1$ transitions. We saw, in fact, that, while the behavior of the computed ratio $R(M1) = B(M1, 1^+_{\rm ms} \rightarrow 2^+_2)/B(M1; 1^+_{\rm ms} \rightarrow 0^+_1)$ versus the number of neutrons is consistent with the data, the absolute strength $B(M1; 2^+_{\rm MS} \rightarrow 2^+_1)$ follows a trend which is at variance with the experimental one. A reexamination of the method is therefore needed.

In deformed nuclei, the QPM accounts for the large number of 0^+ levels observed in several nuclei of rare-earth and actinide regions. It is able to reproduce the distribution of the two-nucleon transfer strength and disclose the phonon composition of each state as well as the quasiparticle structure of each phonon component. The conclusion emerging from such a study is that most of the 0^+ states are mainly one-phonon states built of $q\bar{q}$ pairing correlated configurations. Among them, only one phonon is pairing collective indicating that these 0^+ states describe a pairing vibrational oscillation.

The QPM analysis of the $E2$ and $E0$ transitions indicates that quadrupole collectivity is lacking in all 0^+ states. Given the scarcity of data, however, reliable conclusions may be drawn only after additional systematic measurements of $E2$ and $E0$ decay strengths.

States with $J^\pi = 2^+$ and higher spin were also produced in large abundance. Their properties are satisfactorily described with the QPM.

In conclusion, the QPM proved to be a precious tool for studying the fine structure of collective excitations in vibrational and well-deformed nuclei and disclosing the phonon and quasiparticle composition of the low-lying states. Due to its flexibility, it may be used for

reliable systematics in entire nuclear regions. Embedded in the IBM formalism, it may be used to explore the properties of nuclei in the transitional regions not easily accessible to microscopic approaches. Combining QPM and IBM represents a very promising route which deserves to be explored further.

Acknowledgments

One of the authors (CS) acknowledges the financial support within the agreement between the INFN and the Bulgarian Science Foundation and under the DAAD-08 German and DAAD-09 Bulgarian contracts. VYP acknowledges support by the DFG through grant SFB 634.

References

[1] Bohr A and Mottelson B R 1975 *Nuclear Structure* vol 2 (New York: Benjamin)
[2] Kneissl U, Pitz H H and Zilges A 1996 *Prog. Part. Nucl. Phys.* **37** 439
[3] Kneissl U, Pietralla N and Zilges A 2006 *J. Phys. G: Nucl. Part. Phys.* **32** R217
[4] Pietralla N, von Brentano P and Lisetskiy A F 2008 *Prog. Part. Nucl. Phys.* **60** 225
[5] Frascaria N 1988 *Nucl. Phys.* A **482** 245c
[6] Auman T, Bortignon P F and Hemling H 1998 *Annu. Rev. Nucl. Part. Sci.* **48** 351
[7] Arima A and Iachello F 1984 *Adv. Nucl. Phys.* **13** 139
[8] Rowe D J 1970 *Nuclear Collective Motion: Models and Theory* (London: Methuen)
[9] Ring P and Schuck P 1980 *The Nuclear Many/Body Problem* (New York: Springer)
[10] Bortignon P F, Bracco A and Broglia R A 1998 *Giant Resonances* (Amsterdam: Harwood Academic Publishers)
[11] Sawicki J 1962 *Phys. Rev.* **126** 2231
[12] Yannouleas C, Dworzecka M and Griffin J J 1983 *Nucl. Phys.* A **397** 239
[13] Yannouleas C 1987 *Phys. Rev.* C **35** 1159
[14] Rowe D J 1968 *Rev. Mod. Phys.* **40** 153
[15] Schwesinger B and Wambach J 1984 *Phys. Lett.* B **134** 29
[16] Schwesinger B and Wambach J 1984 *Nucl. Phys.* A **426** 253
[17] Papakonstantinou P and Roth R 2009 *Phys. Lett.* B **671** 356
[18] Dehesa J S, Krewald S, Speth J and Faessler A 1977 *Phys. Rev.* C **15** 1858
[19] Bortignon P F and Broglia R A 1981 *Nucl. Phys.* A **371** 405
[20] Bertsch G F, Bortignon P F and Broglia R A 1983 *Rev. Mod. Phys.* **55** 287
[21] Wambach J, Mishra V K and Chu-Hsia L 1981 *Nucl. Phys.* A **380** 285
[22] Severyukhin A P, Voronov V V and Van Giai N 2004 *Eur. Phys. J.* A **22** 397
[23] Gambacurta D, Grasso M and Catara F 2010 *Phys. Rev.* C **81** 054312
[24] Gambacurta D, Grasso M and Catara F 2011 *Phys. Rev.* C **84** 034301
[25] Litvinova E, Ring P and Tselyaev V I 2007 *Phys. Rev.* C **75** 064308
[26] Litvinova E, Ring P and Vretenar D 2007 *Phys. Lett.* B **647** 111
[27] Kamerdzhiev S, Speth J and Tertychny G 2004 *Phys. Rep.* **393** 1
[28] Tselyaev V I 1989 *Yad. Fiz.* **50** 1252
Tselyaev V I 1989 *Sov. J. Nucl. Phys.* **50** 780
[29] Tselyaev V I 2007 *Phys. Rev.* C **75** 024306
[30] Litvinova E, Ring P and Tselyaev V I 2008 *Phys. Rev.* C **78** 014312
[31] Litvinova E, Ring P and Tselyaev V I 2010 *Phys. Rev. Lett.* **105** 022502
[32] Andreozzi F, Knapp F, Lo Iudice N, Porrino A and Kvasil J 2007 *Phys. Rev.* C **75** 044312
[33] Andreozzi F, Knapp F, Lo Iudice N, Porrino A and Kvasil J 2007 *Phys. Rev.* C **78** 054308
[34] Soloviev V G 1992 *Theory of Atomic Nuclei: Quasiparticles and Phonons* (Bristol: Institute of Physics Publishing)
[35] Otsuka T, Arima A and Iachello F 1978 *Nucl. Phys.* A **309** 1
[36] Belyaev S T and Zelevinsky V G 1962 *Nucl. Phys.* **39** 582
[37] Marumori T, Yamamura M and Tokunaga A 1964 *Progr. Theor. Phys.* **31** 1009
[38] Klein A and Marshalek E R 1991 *Rev. Mod. Phys.* **63** 375
[39] Lesher S R *et al* 2002 *Phys. Rev.* C **66** 051305(R)
[40] Wirth H-F *et al* 2004 *Phys. Rev.* C **69** 044310

[41] Bucurescu D *et al* 2006 *Phys. Rev.* C **73** 064309
[42] Meyer D A *et al* 2005 *J. Phys. G: Nucl Part. Phys.* **31** S1399
[43] Meyer D A *et al* 2006 *Phys. Lett.* B **638** 44
[44] Meyer D A *et al* 2006 *Phys. Rev.* C **74** 044309
[45] Lo Iudice N and Stoyanov Ch 2002 *Phys. Rev.* C **65** 064304
[46] Dinh T K, Grinberg M and Stoyanov Ch 1992 *J. Phys. G: Nucl. Part. Phys.* **18** 329
[47] Grinberg M and Stoyanov Ch 1994 *Nucl. Phys.* A **535** 231
[48] Ponomarev V Yu, Stoyanov Ch, Tsoneva N and Grinberg M 1998 *Nucl. Phys.* A **635** 470
[49] Grinberg M, Stoyanov Ch and Tsoneva N 1998 *Phys. Part. Nucl.* **29** 606
[50] Chepurnov V A 1967 *Sov. J. Nucl. Phys.* **6** 955
[51] Takeuchi K and Moldauer P A 1969 *Phys. Lett.* B **28** 384
[52] Gales S, Stoyanov Ch and Vdovin A I 1988 *Phys. Rep.* **166** 125
[53] Belyaev S T 1967 *Sov. J. Nucl. Phys.* **4** 671
[54] Sakamoto H and Kishimoto T 1990 *Phys. Lett.* B **245** 321
[55] Karadjov D, Voronov V V and Catara F 1993 *Phys. Lett.* B **306** 197
[56] Karadjov D, Voronov V V and Catara F 1994 *J. Phys. G: Nucl. Part. Phys.* **20** 1431
[57] Karadjov D, Voronov V V, Catara F, Grinberg M and Severyuhin A P 1998 *Nucl. Phys.* A **643** 259
[58] Catara F, Piccitto G, Sambataro M and Van Giai N 1996 *Phys. Rev.* B **54** 17536
[59] Catara F, Grasso M, Piccitto G and Sambataro M 1998 *Phys. Rev.* B **58** 16070
[60] Nawrocka-Rybarska W, Stoyanova O and Stoyanov Ch 1980 *Yad. Fiz.* **33** 1494
[61] Arima A, Otsuka T, Iachello F and Talmi I 1977 *Phys. Lett.* B **66** 205
[62] Pietralla N, von Brentano P, Casten R F, Otsuka T and Zamfir N V 1994 *Phys. Rev. Lett.* **73** 2962
[63] Pietralla N, von Brentano P, Otsuka T and Casten R F 1995 *Phys. Lett.* B **349** 1
[64] Palchikov Yu V, von Brentano P and Jolos R V 1998 *Phys. Rev.* C **57** 3026
[65] Nikolaeva R, Stoyanov Ch and Vdovin A I 1989 *Eur. Phys. Lett.* **8** 117
[66] Lo Iudice N and Palumbo F 1978 *Phys. Rev. Lett.* **41** 1532
[67] Bohle D, Richter A, Steffen W, Dieperink A E L, Lo Iudice N, Palumbo F and Scholten O 1984 *Phys. Lett.* B **137** 27
[68] Zawischa D 1998 *J. Phys. G: Nucl. Part. Phys.* **24** 683
[69] Lo Iudice N 2000 *Riv. Nuovo Cimento* **23 n 9** 1
[70] Heyde K, von Neumann-Cosel P and Richter A 2010 *Rev. Mod. Phys.* **82** 2365
[71] Hamilton W D, Irbäck A and Elliott J P 1984 *Phys. Rev. Lett.* **53** 2469
[72] Park P, Subber A R H, Hamilton W D, Elliott J P and Kumar K 1985 *J. Phys. G: Nucl. Phys.* **11** L251
[73] Molnár G, Gatenby R A and Yates S W 1988 *Phys. Rev.* C **37** 898
[74] Ahmad S T, Hamilton W D, Van Isacker P, Hamada S A and Robinson S J 1989 *J. Phys. G: Nucl. Part. Phys.* **15** 93
[75] Giannatiempo A, Nannini A, Perego A, Sona P and Maino G 1991 *Phys. Rev.* C **44** 1508
[76] Giannatiempo A, Nannini A, Perego A, Sona P and Cutoiu D 1996 *Phys. Rev.* C **53** 2770
[77] Pignanelli M, Micheletti S, Blasi N, De Leo R, Borghols W T A, Schippers J M, Van der Werf S Y and Harakeh M N 1988 *Phys. Lett.* B **202** 470
[78] De Leo R *et al* 1989 *Phys. Lett.* B **226** 5
[79] De Leo R, Blasi N, Micheletti S, Pignanelli M, Harakeh M N, Borghols W T A, Schippers J M and Van der Werf S Y 1989 *Phys. Lett.* B **226** 202
[80] De Leo R *et al* 1996 *Phys. Rev.* C **53** 2718
[81] Lieb K P, Börner H G, Dewey M S, Jolie J, Robinson S J, Ulbig S and Winter C 1988 *Phys. Lett.* B **215** 50
[82] Vermeer W J, Lim C S and Spear R H 1988 *Phys. Rev.* C **38** 2982
[83] Hartung G, Richter A, Spamer E, Wörtche H, Rangacharyulu C, de Jager C W and de Vries H 1989 *Phys. Lett.* B **221** 109
[84] Fazekas B, Belgya T, Molnàr G, Veres A, Gatenby R A, Yates S W and Otsuka T 1992 *Nucl. Phys.* A **548** 249
[85] Vanhoy J R, Anthony J M, Haas B M, Benedict B H, Meehan B T, Hicks S F, Davoren C M and Lundstedt C L 1995 *Phys. Rev.* C **52** 2387
[86] Garrett P E, Lehmann H, McGrath C A, Yeh M and Yates S W 1996 *Phys. Rev.* C **54** 2259
[87] Wiedenhöver I, Gelberg A, Otsuka T, Pietralla N, Gableske J, Dewald A and von Brentano P 1997 *Phys. Rev.* C **56** R2354
[88] Hicks S F, Davoren C M, Faulkner W M and Vanhoy J R 1998 *Phys. Rev.* C **57** 2264
[89] Pietralla N *et al* 1998 *Phys. Rev.* C **58** 796
[90] Pietralla N *et al* 1999 *Phys. Rev. Lett.* **83** 1303

[91] Pietralla N, Fransen C, von Brentano P, Dewald A, Fitzler A, Friessner C and Gableske J 2000 *Phys. Rev. Lett.* **84** 3775
[92] Fransen C, Pietralla N, von Brentano P, Dewald A, Gableske J, Gade A, Lisetskiy A and Werner V 2001 *Phys. Lett.* B **508** 219
[93] Fransen C *et al* 2003 *Phys. Rev.* C **67** 024307
[94] Pietralla N *et al* 2001 *Phys. Rev.* C **64** 031301
[95] Gade A, Klein H, Pietralla N and von Brentano P 2002 *Phys. Rev.* C **65** 054311
[96] Lisetskiy A F, Pietralla N, Fransen C, Jolos R V and von Brentano P 2000 *Nucl. Phys.* A **677** 100
[97] Werner V *et al* 2002 *Phys. Lett.* B **550** 140
[98] Klein H, Lisetskiy A F, Pietralla N, Fransen C, Gade A and von Brentano P 2002 *Phys. Rev.* C **65** 044315
[99] Bandyopadhyay D, Reynolds C C, Fransen C, Boukharouba N, McEllistrem M T and Yates S W 2003 *Phys. Rev.* C **67** 034319
[100] Fransen C, Werner V, Bandyopadhyay D, Boukharouba N, Lesher S R, McEllistrem M T, Jolie J, Pietralla N, von Brentano P and Yates S W 2005 *Phys. Rev.* C **71** 054304
[101] Yates S W 2005 *J. Rad. Nucl. Chem.* **265** 291
[102] Gade A, Wiedenhöver I, Gableske J, Gelberg A, Meise H, Pietralla N and von Brentano P 2000 *Nucl. Phys.* A **665** 268
[103] Li T C *et al* 2005 *Phys. Rev.* C **71** 044318
[104] Rainovski G, Pietralla N, Ahn T, Lister C J, Janssens R V F, Carpenter M P, Zhu S and Barton III C J 2006 *Phys. Rev. Lett.* **96** 122501
[105] Ahn T, Pietralla N, Rainovski G, Costin A, Dusling K, Li T C, Linnemann A and Pontillo S 2007 *Phys. Rev.* C **75** 014313
[106] Hicks S F, Vanhoy J R and Yates S W 2008 *Phys. Rev.* C **78** 054320
[107] Ahn T, Coquard L, Pietralla N, Rainovski G, Costin A, Janssens R V F, Lister C J, Carpenter M P, Zhu S and Heyde K 2009 *Phys. Lett* B **679** 19
[108] Rainovski G *et al* 2010 *Phys. Lett* B **683** 11
[109] Coquard L *et al* 2009 *Phys. Rev.* C **80** 061304(R)
[110] Coquard L *et al* 2010 *Phys. Rev.* C **82** 024317
[111] Sieja K, Nowacki F, Langanke K and Martinez-Pinedo G 2009 *Phys. Rev.* C **79** 064310
[112] Sieja K, Martinez-Pinedo G, Coquard L and Pietralla N 2009 *Phys. Rev.* C **80** 054311
[113] Bianco D, Andreozzi F, Lo Iudice N, Porrino A and Knapp F 2011 *Phys. Rev.* C **84** 024310
[114] Lo Iudice N and Stoyanov Ch 2000 *Phys. Rev.* C **62** 047302
[115] Lo Iudice N and Stoyanov Ch 2004 *Phys. Rev.* C **69** 044312
[116] Lo Iudice N and Stoyanov Ch 2006 *Phys. Rev.* C **73** 037305
[117] Lo Iudice N, Stoyanov Ch and Tarpanov D 2008 *Phys. Rev.* C **77** 044310
[118] Lo Iudice N, Stoyanov Ch and Pietralla N 2009 *Phys. Rev. C* **80** 024311
[119] Burda O *et al* 2007 *Phys. Rev. Lett.* **99** 092503
[120] Walz C, Fujita H, Krugmann A, von Neumann-Cosel P, Pietralla N, Ponomarev V Yu, Scheikh-Obeid A and Wambach J 2011 *Phys. Rev. Lett.* **106** 062501
[121] Obeid A S, Burda O, Chernykh M, Krugmann A, von Neumann-Cosel P, Pietralla P, Poltoratska I, Ponomarev V and Walz C 2010 *J. Phys.: Conf. Ser.* **205** 012040
[122] Baker F T *et al* 1983 *Nucl. Phys.* A **393** 283
[123] Franey M A and Love W G 1985 *Phys. Rev.* C **31** 488
[124] Raynal J 2007 *code DWBA07*
[125] Heisenberg J and Blok H P 1983 *Annu. Rev. Nucl. Part. Sci.* **33** 569
[126] von Garrel H *et al* 2006 *Phys. Rev.* C **73** 054315
[127] Jolos R V, Pietralla N, Shirikova N Yu and Voronov V V 2011 *Phys. Rev.* C **84** 014315
[128] Leistenschneider A *et al* 2001 *Phys. Rev. Lett.* **86** 5442
[129] Ryezayeva N *et al* 2002 *Phys. Rev. Lett.* **89** 272502
[130] Adrich P *et al* 2005 *Phys. Rev. Lett.* **95** 132501
[131] Schwengner R *et al* 2007 *Phys. Rev.* C **76** 034321
[132] Klimkiewicz A *et al* 2007 *Phys. Rev.* C **76** 051603(R)
[133] Savran D *et al* 2008 *Phys. Rev. Lett.* **100** 232501
[134] Wieland O *et al* 2009 *Phys. Rev. Lett.* **102** 092502
[135] Tonchev A P *et al* 2010 *Phys. Rev. Lett.* **104** 072501
[136] Tamii A *et al* 2011 *Phys. Rev. Lett.* **107** 062502
[137] Tsoneva N, Lenske H and Stoyanov Ch 2004 *Phys. Lett.* B **586** 213
[138] Tsoneva N and Lenske H 2008 *Phys. Rev.* C **77** 024321

[139] Guhr T, Hummel K D, Kilgus G, Bohle D, Richter A, de Jager C W, de Vries H and de Witt Huberts P K A 1989 *Nucl. Phys.* A **501** 95
[140] Zilges A, von Brentano P, Friedrichs H, Heil R D, Kneissl U, Lindenstruth S, Pitz H H and Wesselborg C 1991 *Z. Phys.* A **340** 155
[141] Fransen C *et al* 1998 *Phys. Rev.* C **57** 129
[142] Robinson S J, Jolie J, Börner H G, Schillebeeckx P, Ulbig S and Lieb K P 1994 *Phys. Rev. Lett.* **73** 412
[143] Wilhelm M, Radermacher E, Zilges A and von Brentano P 1996 *Phys. Rev.* C **54** R449
[144] Wilhelm M, Kasemann S, Pascovici G, Radermacher E, von Brentano P and Zilges A 1998 *Phys. Rev.* C **57** 577
[145] Babilon M, Hartmann T, Mohr P, Vogt K, Volz S and Zilges A 2002 *Phys. Rev.* C **65** 037303
[146] Pietralla N 1999 *Phys. Rev.* C **59** 2941
[147] Grinberg M, Stoyanov Ch and Tsoneva N 1998 *Phys. Part. Nucl.* **29** 606
[148] Metzger F R 1976 *Phys. Rev.* C **14** 543
[149] Metzger F R 1978 *Phys. Rev.* C **18** 2138
[150] Eckert T *et al* 1997 *Phys. Rev.* C **56** 1257
[151] Voronov V V, Thoa D T and Ponomarev V Yu 1984 *Bull. Acad. Sci. USSR Phys. Ser.* **48** 190
[152] Kneissl U 2005 *Proc. 8th Int. Spring Seminar Nuclear Physics* (Singapore: World Scientific) p 399
[153] Smirnova N A, Pietralla N, Mizusaki T and Van Isacker P 2000 *Nucl. Phys.* A **678** 235
[154] Pietralla N, Fransen C, Gade A, Smirnova N A, von Brentano P, Werner V and Yates S W 2003 *Phys. Rev.* C **68** 031305(R)
[155] Jolos R V, Shirikova N Yu and Voronov V V 2004 *Phys. Rev.* C **70** 054303
[156] Jolos R V, Shirikova N Yu and Voronov V V 2006 *Eur. Phys. J.* A **29** 147
[157] Grinberg M, Stoyanov Ch and Tsoneva N 1998 *Part. Nucl.* **29** 1456
[158] Vanhoy J R, Anthony J M, Haas B M, Benedict B H, Meehau B T, Hicks S F, Davoren C M and Lundstedt C L 1995 *Phys. Rev.* C **52** 2387
[159] Ponomarev V Yu, Stoyanov Ch, Tsoneva N and Grinberg M 1998 *Nucl. Phys.* A **635** 470
[160] Ponomarev V Yu 1999 *Eur. Phys. J.* A **6** 243
[161] Tsoneva N, Lenske H and Stoyanov Ch 2004 *Nucl. Phys.* A **731** 273
[162] Iachello F and Jackson A D 1982 *Phys. Lett.* B **108** 151
[163] Zamfir N V *et al* 1997 *Phys. Rev.* C **55** R1007
[164] Soloviev V G, Sushkov A V, Shirikova N Yu and Lo Iudice N 1996 *Nucl. Phys.* A **600** 155
[165] Soloviev V G, Sushkov A V and Shirikova N Yu 1997 *Phys. Rev.* C **56** 2528
[166] Lo Iudice N 1997 *Phys. Part. Nucl.* **28** 556
[167] Soloviev V G, Sushkov A V and Shirikova N Yu 2000 *Phys. Part. Nucl.* **31** 385
[168] Garrett P E 2001 *J. Phys. G: Nucl. Part. Phys.* **27** R1
[169] Zamfir N V, Zhang Jing-ye and Casten R F 2002 *Phys. Rev.* C **66** 057303
[170] Sun Y, Aprahamian A, Zhang J and Lee C 2003 *Phys. Rev.* C **68** 061301(R)
[171] Lo Iudice N, Sushkov A V and Shirikova N Yu 2004 *Phys. Rev.* C **70** 064316
[172] Lo Iudice N, Sushkov A V and Shirikova N Yu 2005 *Phys. Rev.* C **72** 034303
[173] Lo Iudice N and Sushkov A V 2008 *Phys. Rev.* C **78** 054304
[174] Bes D R and Broglia R A 1966 *Nucl. Phys.* **80** 289
[175] Broglia R A, Hansen O and Riedel C 1973 *Advances in Nuclear Physics* vol 6 (New York: Plenum) p 287
[176] Härtlein T, Heinebrodt M, Schwalm D and Fahlander C 1998 *Eur. Phys. J.* A **2** 253
[177] Davidson W F *et al* 1981 *J. Phys. G: Nucl. Phys.* **7** 455
[178] Lehmann H, Jolie J, Corminboeuf F, Börner H G, Doll C, Jentschell M, Casten R F and Zamfir N V 1998 *Phys. Rev.* C **57** 569
[179] Wood J L, Zganjar E F, De Coester C and Heyde K 1999 *Nucl. Phys.* A **651** 323
[180] Akovali Y A 1992 *Nucl. Data Sheets* **66** 505
[181] Abdulvagabova S K, Ivanova S P and Pyatov N I 1972 *Phys. Lett.* B **38** 215
[182] Levon A I *et al* 2009 *Phys. Rev.* C **79** 014318